Biogenic isoprene emissions, dry deposition velocity and surface ozone concentration during summer droughts, heatwaves and normal conditions in Southwestern Europe

Antoine Guion[1*], Solène Turquety[1**], Arineh Cholakian[2], Jan Polcher[2], Antoine Ehret[1], and Juliette Lathière[3]

[1]LMD/IPSL, Sorbonne Université, ENS, PSL Université, École polytechnique, Institut Polytechnique de Paris, CNRS, Paris, France.
[*]Now at INERIS, Verneuil-en-Halatte, France
[**]Now at LATMOS/IPSL, Sorbonne Université, UVSQ, CNRS, Paris, France
[2]LMD/IPSL, École polytechnique, Institut Polytechnique de Paris, ENS, PSL Université, Sorbonne Université, CNRS, Palaiseau, France
[3]LSCE/IPSL, CEA-CNRS-UVSQ, Université Paris-Saclay, Gif-sur-Yvette, France

Correspondence: Antoine Guion (antoine.guion@ineris.fr)

Abstract. At high concentration, tropospheric ozone (O_3) deteriorates air quality, inducing adverse effects on human and ecosystem health. Meteorological conditions are key to understand the variability of O_3 concentration, especially during extreme weather events. In addition to modifying photochemistry and atmospheric transport, droughts and heatwaves affect the state of vegetation and thus the biosphere-troposphere interactions that control atmospheric chemistry, namely biogenic emissions of precursors and ~~gaz~~ gas dry deposition. A major source of uncertainty and inaccuracy in the simulation of surface O_3 during droughts and heatwaves is the poor representation of such interactions. ~~Based on the biogenic emission model MEGANv2.1 and the chemistry-transport model CHIMERE v2020r1, the first objective of this study is to assess the sensitivity of biogenic~~ This publication aims at quantifying the isolated and combined impacts of both extremes on biogenic isoprene (C_5H_8) emissions, O_3 dry deposition and surface O_3 ~~to biomass decrease and soil dryness effect (from several configurations) during the extremely dry summer 2012. Secondly, this research aims at quantifying the variation of observed (EEA's air quality database, 2000-2016) and simulated (CHIMERE, 2012-2014)~~ in Southwestern Europe.

First, the sensitivity of biogenic C_5H_8 emissions, O_3 dry deposition and surface O_3 ~~during summer heatwaves and agricultural droughtsthat have been identified using the Percentile Limit Anomalies (PLA) method. Our sensitivity analysis shows that~~ to two specific effects of droughts, the decrease in ~~both~~ soil moisture and ~~biomass parameter during droughts induces~~ in biomass, is analyzed for the extremely dry summer 2012 using the biogenic emission model MEGANv2.1 and the chemistry-transport model CHIMEREv2020r1. Despite a significant decrease in biogenic C_5H_8 emissions and O_3 dry deposition velocity~~. We find a larger impact induced by the variation of the soil moisture parameter. However, combined effects~~, characterized by a large spatial variability, the combined effect on surface O_3 concentration ~~remain limited . Based on a cluster approach using the PLA indicator, we show that observed O_3 concentration is on average significantly higher during heatwaves (~~remains limited (between +~~18μg/m³ in daily maximum) and droughts (0.5%~~ and +~~9μg/m³)compared to normal conditions. Despite a~~

difference of several $\mu g/m^3$, CHIMERE correctly simulates the variations of 3% over the continent).

The variations of simulated biogenic C_5H_8 emissions, O_3 dry deposition and surface O_3 during the heatwaves and agricultural droughts are then analyzed for summer 2012 (warm and dry), 2013 (warm) and 2014 (relatively wet and cool). We compare the results with large observational data sets: O_3 concentrations from Air Quality e-Reporting (2000-2016) and total columns of formaldehyde ($HCHO$, used as a proxy of biogenic emissions of volatile organic compounds) from the Ozone Monitoring Instrument of the Aura satellite (2005-2016).

Based on a cluster approach using the Percentile Limit Anomalies indicator, we find that C_5H_8 emissions increase by +33% during heatwaves compared to normal conditions, do not vary significantly during all droughts (accompanied or not by a heatwave) and decrease by -16% during isolated droughts. OMI data confirm an average increase of $HCHO$ during heatwaves (between +15 and +31% depending on the product used) and decrease of $HCHO$ (between -2 and -6%) during isolated droughts over 2005-2016 summers. Simulated O_3 dry deposition velocity decreases by -25% during heatwaves and -35% during all droughts. Simulated O_3 concentrations increase by +7% during heatwaves and by +3% during all droughts. Compared to observations, CHIMERE tends to underestimate the daily maximum O_3. However, similar sensitivity to droughts and heatwaves are obtained. The analysis of the AQ e-Reporting data set shows an average increase of +14% during heatwaves and +7% during all droughts over 2000-2016 summers (for an average daily concentration value of $69\mu g/m^3$ under normal conditions). This suggests that identifying the presence of combined heatwaves is fundamental to the study of droughts on surface-atmosphere interactions and O_3 concentration.

1 Introduction

Tropospheric ozone (O_3) plays a critical role in maintaining the oxidative capacity of the troposphere. However, as a high oxidant, it also deteriorates air quality at high concentrations, inducing adverse effects on human and ecosystem health. Both short and long-term O_3 exposure significantly increase the risk of morbidity and mortality from cardiovascular or respiratory causes (e.g. Jerrett et al., 2009; Nuvolone et al., 2018). It also causes visible damage on plant epidermis as well as photosynthesis inhibition, seriously threatening vegetation growth (Anand et al., 2021) and crop yields (De Andrés et al., 2012). Tai et al. (2014) estimate that O_3 pollution enhanced by global warming (Representative Concentration Pathway 8.5) could lead to a global crop yield reduction by 3.6% in 2050.

Tropospheric O_3 is a secondary air pollutant formed by photochemical reaction chains initiated by the oxidation of volatile organic compounds ($VOCs$) in the presence of nitrogen oxides (NO_x). VOC/NO_x emission ratio determines the chemical

regime of O_3 production at local scale in a highly nonlinear relationship (Jacob, 1999). Methane (CH_4) and carbon monoxide

55   (CO) are also O_3 precursors in background conditions.

Meteorological conditions are a key driver for O_3 formation and transport (Mertens et al., 2020). Indeed, O_3 production is favoured by warm and sunny conditions, and O_3 peaks therefore occur mainly during summer. The overall objective of this paper is to quantify the variation of surface O_3 concentrations over the Euro-Mediterranean area during extreme weather events of heatwaves and droughts. The Euro-Mediterranean region is often affected by both heatwaves (Russo et al., 2015) and droughts

60   (Spinoni et al., 2015). The intensity and frequency of such events have increased over the last decades in the region. According to projections based on climate models, these trends could last and worsen over the 21st century (Perkins-Kirkpatrick and Gibson, 2017; Spinoni et al., 2018).

Heatwaves are often associated with high O_3 concentration. For example, Vautard et al. (2005) show that the persistent heatwave of August 2003 led to high O_3 concentration over the Western Europe for several days (daily maximum above $150\mu g/m^3$,

65   spatially averaged). Jaén et al. (2021) report hourly values of O_3 exceeding $250\mu g/m^3$ during a shorter heatwave (28-29 June 2019) at local scale (Barcelona). These values are well above the European Union (EU) recommendation of a 8h-average maximum of $120\mu g/m^3$.

Porter and Heald (2019) highlight that despite a strong correlation between surface temperature and O_3 concentration identified in Europe, this relationship is nonlinear and complex as it depends on several mechanisms including precursor emissions,

70   reaction rates and lifetimes in the atmosphere. High temperatures favour emissions of biogenic $VOCs$ ($BVOCs$), which can induce an increasing formation of O_3 in the case of a NO_x-limited regime as many areas in the Mediterranean basin (Richards et al., 2013). Persistent and intense solar radiation also allows long photochemical episodes (Jaén et al., 2021). Heatwaves in the Mediterranean being often related to a blocking situation of atmospheric systems, stagnant anticyclonic conditions lead to the accumulation of both precursors and O_3 (Otero et al., 2021). Moreover, extreme temperature and high O_3 concentration

75   can cause stomatal closure reducing the dry deposition of O_3, as highlighted by Gong et al. (2020) with the O_3-vegetation feedback.

Droughts also significantly impact atmospheric chemistry through biosphere and atmospheric cycle perturbation (Wang et al., 2017). Drought impact on air pollutants and more specifically O_3 is difficult to investigate for several reasons. It is firstly related to their characterization. Due to their multiscalar character, droughts can last on timescales ranging from days to months,

80   making their extent difficult to assess (Vicente-Serrano et al., 2010). Moreover, drought definition depends on the type considered (Svoboda and Fuchs, 2016). Meteorological droughts correspond to a rainfall deficit or an excess of evapotranspiration, agricultural ones to soil water shortage for plant growth (soil dryness), and hydrological ones to surface and/or underground flow decrease. Another difficulty is that droughts affect not only the atmosphere but also the land biosphere through soil dryness and plant activity decline (e.g. Vicente-Serrano, 2007; Vicente-Serrano et al., 2013).

85   The variability of O_3 concentration is generally not well represented in chemistry-transport models (CTMs) compared to observations partially because of the lack of interactions between the meteorology, terrestrial biosphere and atmospheric chemistry (Wang et al., 2017). Uncertainties related to BVOC emission modelling could lead to a BVOC-derived O_3 uncertainty estimated at about 50% in Europe (Curci et al., 2010). Another major cause of uncertainties concerns the simulation of meteorological

conditions.

90 Meteorological conditions specific to droughts are low relative humidity, low or absence of precipitation and cloud cover. The latter leads to an increase of downward solar radiation. Temperature can also be higher during droughts than during normal conditions. Wang et al. (2017) found that drought periods in the United States over 1990-2014 were characterized by temperatures up to $2°C$ hotter and radiation $12.4W/m^2$ higher. Their analysis of surface measurements shows a mean enhancement in O_3 concentration of 3.5 ppbv (8%), explained by enhanced precursor emissions and photochemistry. Finally, large amount

95 of O_3 precursors emitted during biomass burning enhanced by droughts and heatwaves, can contribute to O_3 pollution peaks (e.g. Hodnebrog et al., 2012).

The development of droughts and heatwaves can be linked (Miralles et al., 2019). For example, through the soil moisture-temperature feedback, droughts can increase heatwave intensity due to a decrease in evapotranspiration and an increase in sensible heat (e.g. Zampieri et al., 2009). It is therefore important to integrate such interactions for the simulation of droughts

100 and heatwaves.

Through soil moisture deficit, droughts can induce considerable adverse effects on the biosphere, leading to a decrease of the overall biomass but also of the BVOC emission activity. Guion et al. (2021) report an averaged decrease of $\sim 10\%$ of Leaf Area Index (LAI) observed by satellite during droughts in Southern Europe. Areas of low altitude and vegetation with short root systems are more sensitive. Based on simulations from the Model of Emissions of Gases and Aerosols from Nature (MEGAN)

105 (Guenther et al., 2006, 2012) and using MODIS LAI between 2003 and 2018, Cao et al. (2021) find that vegetation biomass variability in China is a major controlling factor of the inter-annual variation of BVOC emissions. Furthermore, Emmerson et al. (2019) simulated (also with MEGAN) a reduction in C_5H_8 emissions of 24-52% over Southeastern Australia due to soil dryness in summer.

Dry deposition velocity in the Mediterranean depends on both stomatal and non-stomatal conductance (Lin et al., 2020; Sun

110 et al., 2022). Stomatal conductance that can be considerably affected under hot and dry conditions, depends on several parameters. As identified by Kavassalis and Murphy (2017), the leaf-to-air vapor pressure deficit that depends on both temperature and relative humidity, is a key variable regulating the stomatal conductance. Extreme hot and dry conditions can cause stomatal closure to reduce transpiration. Moreover, lack of rainfall prevents wet deposition and plant water stress slows dry deposition. However, there are still large uncertainties about the relationship between the soil moisture and the ~~gaz~~ gas dry deposition (e.g.

115 Clifton et al., 2020b).

Considering the difficulty for models to simulate accurately soil moisture (Cheng et al., 2017) and the uncertainties about plant and BVOC species response to water stress (Bonn et al., 2019), the impact of soil moisture is often dismissed in biogenic emissions and dry deposition schemes used in CTMs. Therefore, knowledge about the respective effect on O_3 remains limited. To evaluate the effects of droughts and heatwaves on surface O_3 in Southwestern Europe, the variation of both BVOC emissions

120 and dry deposition as a function of meteorological and hydrological conditions are analyzed in this paper including the soil dryness effect.

Agricultural droughts and heatwaves are identified based on the coupled meteorological and land surface vegetation regional model RegIPSL for the 1979-2016 period (Guion et al., 2021). Summers are less affected by drought events (33% of them) than

by heatwaves (97%). Nevertheless, drought periods are generally much longer than heatwaves (22.3 days against 5.8). Those two types of extreme weather events can be considerably correlated over the Western Mediterranean (temporal correlation R between 0.4 and 0.5).

Atmospheric chemistry is simulated using the regional CHIMERE CTM (Menut et al., 2021) over three selected summers (2012, 2013 and 2014), including the online calculation of biogenic emissions from the MEGANv2.1 model. Simulations are analyzed in conjunction with surface O_3 observations from the European surface network Air Quality e-Reporting (https://www.eea.europa.eu/data-and-maps/data/aqereporting-9). Concentrations of formaldehyde ($HCHO$) are used as a proxy for BVOC emissions. $HCHO$ is produced in high yield during the oxidation of hydrocarbons. As an intermediate product of the oxidation of most VOC and being characterized by a short lifetime (about a few hours), $HCHO$ has been used in many studies to infer VOC emissions (e.g. Millet et al., 2006, 2008; Curci et al., 2010). Observations of $HCHO$ total column by the Ozone Monitoring Instrument (OMI) onboard the Aura satellite (Levelt et al., 2006) are used.

The observations and models used for this research are presented in Sect. 2 and 3, respectively. The RegIPSL, CHIMERE and MEGAN models, as well as the different modelling experiments undertaken are detailed. Validation of surface O_3, NO_2 and 2m temperature are presented in Sect. 4. Results (see Sect. 5) are divided into three parts. Firstly, the sensitivity of C_5H_8 emissions, O_3 dry deposition and surface O_3 concentration to drought effects (biomass decrease and soil dryness) is assessed in Sect. 5.1. Secondly, the variation of observed and simulated O_3, integrating drought and heatwave effects, is analyzed with respect to the variation of troposphere-atmosphere interactions during extreme weather events (see Sect. 5.2). Finally, the number and distribution of days exceeding the EU air quality standard are presented (see Sect. 5.3).

2 Observations

2.1 European surface network of O_3 and NO_2 concentration

The in-situ measurements of surface O_3 and NO_2 provided by the European Environment Agency are used (EEA, https://www.eea.europa.eu/data-and-maps/data/aqereporting-9, last access: 30 July 2021). The AQ e-Reporting project gathers air quality data provided by EEA member countries as well as european collaborating countries. Merging with the statistics of AirBase v8 project (2000-2012), AQ e-Reporting offers a multi-annual time series of air quality measurement data until 2021, categorized by station types and zones across Europe. Only measurements from stations classified as background and rural are considered for this study.

Thunis et al. (2013) quantify the various sources of uncertainty for O_3 measurements (e.g. linear calibration and ultraviolet photometry) and estimated a total uncertainty of 15%, regardless of concentration level. There are also considerable uncertainties in the measurements of NO_2. Lamsal et al. (2008) emphasize that the chemiluminescence analyzer, the measurement technique primarily found in air quality stations, is subject to significant interference from other reactive species containing oxidized nitrogen (e.g. PAN, HNO_3). This can lead to an overestimation of measured NO_2 concentrations.

2.2 Satellite observations of $HCHO$ total column

The $HCHO$ total column retrieved from the observations of the backscatter solar radiation in the ultraviolet (306 and 360 nm) by the OMI/Aura instrument are used as a quantitative proxy of BVOC emissions. OMI has an equator crossing time at 01:45 pm on the ascending node, about 14.5 revolutions per day and a swath width of 2600 km, allowing daily global coverage (Levelt et al., 2006, 2018).

Uncertainties on the $HCHO$ retrieval is significant, varying between 30% (pixels with high concentrations) and 100% (with low concentrations), mainly due to cloud and aerosol scattering along the field of view (González Abad et al., 2015). Satellite retrievals of $HCHO$ have been shown to have systematic low mean bias (20-51%) compared to aircraft observations (Zhu et al., 2016).

For this reason, we chose to focus on the relative difference in total HCHO during droughts and heatwaves (no correction factor has been applied). In order to quantify the uncertainty on the $HCHO$ anomalies obtained, the analysis has been performed using two products. We primarily use the OMHCHOd level 3 product (Chance, 2019), which provides $HCHO$ total column with a spatial resolution of $0.1° \times 0.1°$. For comparison, the level 2 retrieval by the Belgian Institute for Space Aeronomy (BIRA) is also used (De Smedt et al., 2015), thereafter referred to as OMI-BIRA. Both products are included in the intercomparison conducted by Zhu et al. (2016).

Only observations with a cloud fraction less than 0.3, a solar zenith angle less than 70° and a vertical column density within the range of -0.8x10^{15} and 7.6x10^{15} $mocelules/cm^2$ are selected in order to minimize OMI row anomalies, following Zhu et al. (2017). For a suitable comparison with model simulations, $HCHO$ data were regridded on the Med-CORDEX domain using a bilinear method.

2.3 In-situ observations of 2m temperature, C_5H_8 surface concentration and O_3 dry deposition flux

To complete the validation of our simulations, several observational data sets are added to our study. Firstly, in-situ observations of temperature at 2 meters above the surface (T_{2m}) from the E-OBS data set (Cornes et al., 2018) are used to validate the simulated temperature by the Weather Research and Forecasting (WRF) model (Skamarock et al., 2008). The E-OBS gridded product with a resolution of $0.25° \times 0.25°$ was regridded to the Med-CORDEX domain (see Sect. 3.1.1).

Secondly, flux measurements are used for comparison with the different modelling experiments carried out to analyze the sensitivity of biogenic C_5H_8 emissions and O_3 deposition to the effects of biomass decrease and soil dryness. However, there are few flux measurements available that cover at least several weeks during summer 2012. The ERSA station (FR0033R), located at Cape Corsica in France (42.97°N, 9.38°E) is used to assess surface concentration of C_5H_8 measured by a steel canister instrument at 4.0 meters above the surface. The data are provided by the EBAS infrastructure (https://ebas.nilu.no/).

Dry deposition flux measurements of O_3 are also used at one station. This is the Castelporziano station (IT-Cp2) located in the Lazio region of Italy (41.70°N, 12.36°E) measuring at 14.9 meters above the surface (eddy covariance technique). A full description of the measurement data is provided in Fares et al. (2013). The data were downloaded from the European Fluxes Database Cluster (EFDC, http://www.europe-fluxdata.eu/).

3 Models

3.1 RegIPSL (WRF-ORCHIDEE)

3.1.1 Model description

The regional WRF-ORCHIDEE model (RegIPSL) couples the land surface model ORCHIDEE (ORganising Carbon and Hydrology In Dynamic EcosystEms) (Maignan et al., 2011) and the meteorological model WRF. ORCHIDEE is composed of three modules; SECHIBA that simulates the water and energy cycle, STOMATE that resolves the processes of the carbon cycle allowing therefore an interactive phenology and finally, LPJ that computes the competition between the Plant Functional Types (PFTs). However, LPJ module is not used for this research.

RegIPSL model has been used following the recommendation of the Med-CORDEX (Coordinated Regional Climate Downscaling Experiment over the Mediterranean domain) initiative (Ruti et al., 2016). On a Lambert-conformal projection, the domain covers the Euro-Mediterranean with a spatial resolution of 20km. The full description of the configuration used with RegIPSL is presented in Guion et al. (2021).

The performed Med-CORDEX simulations over the 1979-2016 period have been evaluated against surface observations of temperature and precipitation, demonstrating that it is suitable for research on droughts and heatwaves (Guion et al., 2021).

3.1.2 Indicators of drought and heatwave

Based on simulations performed by the RegIPSL model, we identified heatwaves and agricultural droughts over the Euro-Mediterranean using indicators of extreme weather events, as described in Guion et al. (2021) (data access: https://thredds-x.ipsl.fr/thredds/catalog/HyMeX/medcordex/data/Droughts_Heatwaves_1979_2016/catalog.html).

Following the approach of Lhotka and Kyselý (2015), we computed the Percentile Limit Anomalies of 2m above surface temperature (PLA_{T2m}) for heatwave detection and of soil dryness (PLA_{SD}) for agricultural drought detection. The soil dryness is computed as the complement of the soil wetness index, which is described in ORCHIDEE as the ratio between the soil moisture and the accesible water content.

For each cell of longitude (i) and latitude (j) of the domain, the monthly distribution of the 2m temperature/soil dryness is normalized and the 75th percentile is computed ($p = 0.75$). The daily $PLA_{T2m/SD}$ indicator is equal to the daily deviation ($dX_{i,j,d}$) between the reference variable ($X_{i,j,d}$) and the corresponding monthly percentile ($X_{i,j,m}^p$) (Equation 1). A heatwave/drought is identified when the daily $PLA_{T2m/SD}$ is positive for three consecutive days.

$$dX_{i,j,d} = X_{i,j,d} - X_{i,j,m}^p \tag{1}$$

The chosen percentile for the detection of extreme weather events is generally higher, between 80 and 95 (e.g. Stéfanon et al., 2012). We chose the percentile 75 in this study for a larger population. As a result, events detected here cover not only extreme events, but also periods that are significantly drier and warmer than normal conditions.

PLA_{T2m} was calculated based on 2m temperature observations (E-OBS data set) in Guion et al. (2021). Although the intensity of heatwaves was slightly overestimated with the Med-CORDEX simulations (+0.16°C for the mean bias and +0.50°C for the maximum bias), their temporal correlation with observations was high (R coefficient of about 0.9 over the whole Mediterranean).

3.1.3 Soil water stress for plants

The Soil Water Stress (SWS) calculated by RegIPSL is used to describe the water stress for plant transpiration and photosynthesis (de Rosnay et al., 2002). It is an index varying between 0 (plants fully stressed) and 1 (not stressed) that takes into account the water transfer between the soil layers along root profiles (11 layers in the version of ORCHIDEE used here). For each PFT (p), soil class (s) and soil layer (v), it is computed as follows:

$$SWS_{p,s} = \frac{SM_{p,s,v} - SMw_{p,s,v}}{SMnostress_{p,s,v} - SMw_{p,s,v}} \times nroot_{p,s,v} \tag{2}$$

where SM is the soil moisture (liquid phase), SMw the level at wilting point, $SMnostress$ the level at which SWS reaches 1 and $nroot$ the normalized root length fraction in each soil layer (between 0 and 1). There are three soil classes to avoid competition for water uptake: bare soil, soil with short root systems and soil with long ones.

3.2 CHIMERE

3.2.1 Model description and configuration

The CHIMERE v2020r1 Eulerian 3-dimensional regional CTM (Menut et al., 2021) computes gas-phase chemistry, aerosol formation, transport and deposition. It can be guided by pre-calculated meteorology (offline simulation) or used in online with the WRF regional meteorological model (Skamarock et al., 2008), including the direct and indirect effects of aerosols in option. In this study, we chose to use the online version of CHIMERE but without any aerosol effects in order to reduce the calculation time and to isolate possible feedbacks.

Here, the reduced scheme MELCHIOR2 (Derognat, 2003) is used for gas phase chemistry (44 species, almost 120 reactions). The aerosol module includes aerosol microphysics, secondary aerosol formation mechanisms, aerosol thermodynamics and deposition, as detailed in Couvidat et al. (2018); Menut et al. (2021). The photolysis rates are calculated online using the Fast-JX module version 7.0b (Bian and Prather, 2002) which accounts for the radiative impact of aerosols.

The WRF model used with CHIMERE, which has a different configuration from the RegIPSL model (Guion et al., 2021), has 15 vertical layers, from 998hPa up to 300hPa. The physics interface for the surface is provided by the Noah Land Surface Model. The aerosol-aware Thompson scheme (Thompson and Eidhammer, 2014) is used for the mycrophysics parameterization. Horizontal and vertical advection are based on the scheme of Van Leer (1977). The reanalysis meteorological data for the initial and boundary conditions are provided by the National Centers of Environmental Prediction (NCEP). The physical and chemical time steps are respectively 30 and 10 minutes.
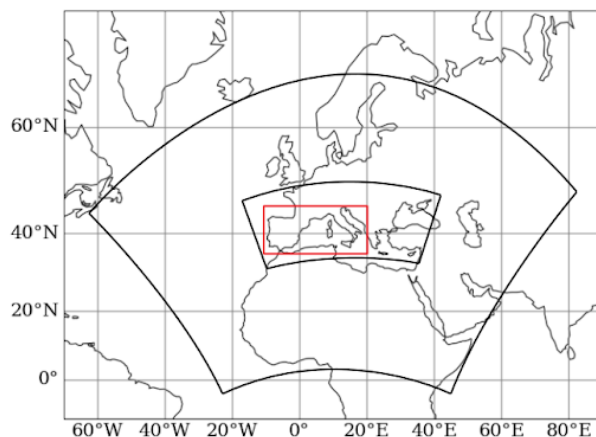
Figure 1. Domains used for the CHIMERE simulations: EUMED60 at 60km resolution is the large domain, the smaller nested domain is Med-CORDEX at 20km resolution. The Southwestern Europe region studied here is shown in red.

The simulations have been performed for June-July-August (with a 5 days spin-up) of years 2012-2013-2014 over two nested simulation domains (Fig. 1). The large domain covers Northern Africa and Europe at 60km horizontal resolution (EUMED60, 164x120 cells) and the small domain is close to that of Med-CORDEX although smaller; it covers the Western Mediterranean region at 20km horizontal resolution (Med-CORDEX, 222x93 cells). The area studied in more detail in the following is the Southwestern Europe (35-46°N, 10°W-20°E).

Chemical boundary conditions for the larger domain are provided by a climatology from the global CTM LMDZ4-INCA3 (Hauglustaine et al., 2014) for trace gases and non-dust aerosols, and from the GOCART model (Chin et al., 2002) for dust. The biogenic emissions are calculated online by the MEGAN model (see Sect. 3.2.2). Sea salts and dimethyl sulfide marine emissions are calculated online using the scheme of Monahan (1986) and Liss and Mervilat (1986), respectively. Mineral dust emissions are also calculated on-line (Marticorena and Bergametti, 1995; Alfaro and Gomes, 2001). Consistently with the WRF model, the land cover classification used for the calculation of biogenic and dust emissions is from the United States Geological Survey (USGS) land cover database (http://www.usgs.gov). The biomass burning emissions from the APIFLAME v2.0 model (Turquety et al., 2020) are used. The anthropogenic surface emissions are derived from the EMEP database at 0.1°×0.1° resolution (https://www.ceip.at/webdab-emission-database) for the year 2014. The inventory was preprocessed by the emiSURF program in order to calculate hourly emissions fluxes on the CHIMERE grid and the period of simulations (https://www.lmd.polytechnique.fr/chimere/formation_2021/emisurf.pdf).

3.2.2 MEGAN and the soil moisture factor

BVOC emissions were computed using the MEGAN model v2.04 (Guenther et al., 2006), including several updates from the version 2.1 (Guenther et al., 2012). It is used on-line in the CHIMERE model at hourly time step. Emission fluxes are calculated based on emission factors at canopy standard conditions that are defined as $303K$ for the air temperature (T), $1500\ \mu mol/m^2.s$

for the photosynthetic photon flux density ($PPFD$) at the top of the canopy, 5 m^2/m^2 for the LAI and a canopy composed of 80% mature, 10% growing and 10% old foliage. Environmental conditions are taken into account using activity factors (γ) that represent deviations from the canopy standard conditions, so that the emission rate (ER [$\mu g.m^{-2}.h^{-1}$]) for a given species i is calculated in each model grid cell as:

$$ER_i = EF_i \cdot \gamma_{LAI} \cdot \gamma_{PPFD,i} \cdot \gamma_{T,i} \cdot \gamma_{Age,i} \cdot \gamma_{SM,i} \cdot \gamma_{CO2,i} \cdot \rho_i \tag{3}$$

where EF is the emission factor [$\mu g.m^{-2}.h^{-1}$] provided by the MEGAN model and ρ the production/loss term within canopy that is assumed to be equal to 1.

γ_{LAI} is the activity factor based on LAI observations from the MODIS MOD15A2H product (Myneni et al., 2015) improved by Yuan et al. (2011) (http://globalchange.bnu.edu.cn/research/lai). This improvement is undertaken with a two-step integrated method: (1) the Modified Temporal Spatial Filter is used to fill the gaps and replace low quality data by consistent ones; (2) the TIMESAT Salvitzky and Golay filter is applied to smooth the final product. The temporal resolution is 8 days.

γ_{PPFD}, γ_T and γ_{Age} are the activity factors accounting for light, temperature and leaf age respectively. They are calculated in MEGAN using meteorological variables from the WRF model. The activity factors accounting for the soil moisture (γ_{SM}) and CO_2 concentration (γ_{CO2}) are applied on C_5H_8 species only. γ_{CO2} is fixed (CO_2 concentration at 395 ppm) and γ_{SM} depends on the deviation between the soil wetness and a fixed wilting point, computed as follows:

$$
\begin{cases}
\gamma_{SM} = 1 & \text{if } \theta > \theta_1 \\
\gamma_{SM} = \frac{(\theta - \theta_w)}{\Delta\theta_1} & \text{if } \theta_w < \theta < \theta_1 \\
\gamma_{SM} = 0 & \text{if } \theta < \theta_w
\end{cases}
\tag{4}
$$

where θ is the soil wetness (volumetric water content in m^3/m^3), θ_w the wilting point (level from which plants can not extract water from the soil, in m^3/m^3), $\Delta\theta_1$ equal to 0.04 (empirical parameter) and θ_1 the sum of θ_w and $\Delta\theta_1$. θ values (third layer, 60cm depth) are provided by the WRF-Noah land surface model (Ek et al., 2003; Greve et al., 2013). θ_w values are computed over the domain (Supplementary Information: Fig. S1) using tabulated values from Chen and Dudhia (2001) that are soil type specific and parameterized on Noah soil wetness values. These values are spatialized using the soil texture map provided by the USGS (STATSGO-FAO product). However, emission response to drought is very sensitive to the wilting point (Müller et al., 2008). Wang et al. (2021b) computed a relative difference of biogenic emissions varying between 50 and 90% depending on the wilting point values.

Based on a comprehensive data set of in-situ measurements of C_5H_8 emissions, Bonn et al. (2019) computed an activity factor of soil moisture in function of the soil water availability. The fitted function is relatively in good agreement with the γ_{SM} algorithm in MEGAN.

As an alternative, Jiang et al. (2018) propose to use an activity factor of soil moisture that integrates the soil water stress for

plant photosynthesis. Below a critical value (fixed here at 0.5), the activity factor using SWS from RegIPSL (γ_{SWS}) decreases lineary as follows:

$$
\begin{cases}
\gamma_{SWS} = 2\,SWS & \text{if} \;\; SWS \leq 0.5 \\
\gamma_{SWS} = 1 & \text{if} \;\; SWS > 0.5
\end{cases}
\tag{5}
$$

The different soil wetness functions presented here will be subject to dedicated simulations for comparison.

300   Soil NO emissions are also included in the different simulations. Emission factors are based on the European soil emission inventory (Stohl et al., 1996) which includes both contribution from forests and agricultural soils. Due to the strong temperature dependence, activity factors of soil NO are processed as for biogenic emissions in the MEGAN model. However, no dependence on soil moisture was parameterized.

3.2.3   Dry deposition scheme

305   Dry deposition in CHIMERE is resolved online using a canopy resistance approach, based on the scheme of the EMEP model (Wesely, 1989; Emberson et al., 2000; Simpson et al., 2003, 2012). Canopy resistance is calculated from stomatal conductance (g_{sto}) which increases proportionally with LAI, and the bulk non-stomatal conductance (G_{ns}). g_{sto} varies between a maximum (g_{max}) and minimum (g_{min}) daytime stomatal conductance [mmol $O_3/m^2.s$] depending on a series of meteorological conditions represented by factors of relative conductance (f) (Eq. 6). The parameters used to calculate these factors vary with

310   land cover (lc) and the seasonality. Because the land cover classes used in the dry deposition scheme are different from the one used in CHIMERE (USGS), a matrix of conversion is applied.

$$
g_{sto} = g_{max,lc} \cdot f_{phen,lc} \cdot f_{light,lc} \cdot max(g_{min,lc}, (f_{temp,lc} \cdot f_{VPD,lc} \cdot f_{SWS,lc}))
\tag{6}
$$

where f_X are factors of relative conductance determined by the leaf/needle age ($X = phen$), irradiance ($X = light$), temperature ($X = temp$), leaf-to-air vapour pressure deficit ($X = VPD$) and the soil moisture ($X = SWS$). Environmental variables

315   required for f_X factors are from the WRF model except for f_{SWS} that is based on SWS from RegIPSL. f_{SWS} for which the calculation is the same as γ_{SWS}, follows the parameterization suggested by Simpson et al. (2012) for the stomatal conductance. G_{ns} depends on three resistances: the external leaf uptake, the ground surface and the in-canopy. The external leaf uptake resistance is fixed at 2500 s/m, the ground surface resistance is estimated from tabulated values (PFT specific) and the in-canopy resistance varies with the surface area index which is expressed in terms of LAI. The LAI used in the dry deposition scheme is

320   parameterized (with no inter-annual variation). Information on phenology and biomass variation for each land cover type was collected from several studies in Emberson et al. (2000).

3.3 Modelling experiments

The years 2012-2013-2014 were selected for the large diversity of hydro-climatic conditions and the availability of O_3 observations over the study area. During summer 2012, Southwestern Europe was affected by severe droughts ($PLA_{SD} > 0.1$ of
soil dryness) and heatwaves ($PLA_{T2m} > 1.5°C$) (SI: Fig. S2). The summer 2013 was wet in the Iberian Peninsula, while the summer 2014 was wet in Italy and the Balkans. A few heatwaves occurred in summer 2013 over Southern France, Northern Italy and Northern Spain. Summer 2014 was colder (PLA_{T2m} of -4.0°C) for the entire study area. The analysis method we propose here is divided into two steps.

Firstly, a focus is made on drought effects (biomass decrease and soil dryness) that are generally poorly represented in modelling experiments, over summer 2012. Several experiments are conducted on the Med-CORDEX domain in order to analyze the sensitivity of simulated C_5H_8 emissions, O_3 dry deposition and surface O_3 concentration to drought effects. Table 1 summarizes the CHIMERE simulations conducted. The "Reference" simulations include all the emissions as defined in Sect. 3.2.1 but without accounting for the soil moisture factor in the emission scheme of MEGAN and deposition one of CHIMERE. A simulation with no biogenic emissions is also performed ("NoBio-emiss") to estimate their relative contribution to O_3 concentration.

The LAI used in the emission scheme of MEGAN is year dependent (MODIS observations). To evaluate the effect of biomass decrease by droughts, a simulation with LAI corresponding to a wet summer was used ("HighLAI-emiss"). Summer 2012 which was affected by an important biomass decrease over most of the study area (SI: Fig. S3), has been simulated with the LAI of the wet summer of 2014 (higher than the 2012-2014 mean).

The LAI database used in the dry deposition scheme of CHIMERE does not vary with the year, so that the biomass decrease during the summer 2012 is not reflected. In order to evaluate the importance of this effect, a simulation ("LAIdecr-dep") with a LAI decrease of 5% for forests and 20% for grass and crops (close to the variations observed in 2012 (SI: Fig. S3)) has been conducted.

The effect of soil dryness for the BVOC emissions is evaluated using three different approaches:

- using γ_{SM} from WRF-Noah in MEGAN ("γ_{SM}-emiss" experiment),

- using γ_{SWS} from RegIPSL in MEGAN ("γ_{SWS}-emiss" experiment),

- using γ_{SWSfit} from RegIPSL in MEGAN ("γ_{SWSfit}-emiss" experiment). The fitted function of Bonn et al. (2019) is applied on the SWS as follows:

$$\gamma_{SWSfit} = exp(-exp(0.056 \cdot exp(1) \cdot (-2.3 - SWS) + 1)) \tag{7}$$

The soil dryness effect on the dry deposition is evaluated using the f_{SWS} from RegIPSL in CHIMERE ("f_{SWS}-dep" experiment).

Secondly, based on a simulation configuration integrating all drought and heatwave effects ("γ_{SWSfit}-emiss & LAIdecr/f_{SWS}-dep" experiment, hereafter called "all-emiss-dep" experiment), the variation of C_5H_8 emissions, O_3 dry deposition velocity

Table 1. Name, description and aim of the simulations launched with the CHIMERE model on the nested Med-CORDEX domain for summers 2012, 2013 and 2014.

Simulation name	Description	Aim
Reference (R.)	CHIMERE reference (v2020r1)	Default for dry and hot periods
On biogenic emissions		
NoBio-emiss	R. without biogenic emissions	Contribution of biogenic emissions to O_3
HighLAI-emiss	R. with wet summer LAI	Effect of biomass decrease
γ_{SM}-emiss	R. with γ_{SM} factor from Noah	Effect of soil dryness
γ_{SWS}-emiss	R. with γ_{SWS} factor from ORCHIDEE	Effect of soil dryness
γ_{SWSfit}-emiss	R. with γ_{SWSfit} factor from ORCHIDEE	Effect of soil dryness
On gas dry deposition		
LAIdecr-dep	R. with prescribed LAI reduction	Effect of biomass decrease
LAIdecr/f_{SWS}-dep	R. with prescribed LAI reduction and f_{SWS} factor from ORCHIDEE	Effect of biomass decrease and soil dryness

and surface O_3 concentration is analyzed over summers 2012, 2013 and 2014. In order to compare isolated and combined extreme events with normal conditions, we used a cluster approach based on the PLA_{T2m} and PLA_{SD} indicators.

4   Validation of surface O_3, NO_2 and T_{2m}

Simulated surface O_3 and NO_2 concentrations by CHIMERE were compared to the EEA observations while simulated T_{2m} by the WRF model was compared to the E-OBS observations (Cornes et al., 2018). Table 2 presents the mean validation scores of the "Reference" simulations over Southwestern Europe for summer 2012. Validation scores of O_3 and NO_2 are very similar for summers 2013 and 2014.

The simulated surface O_3 is slightly higher than the observations for hourly and daily mean values (bias "observation - model" of -1.93 and -0.13$\mu g/m^3$) and lower for the daily maximum values (+10.94$\mu g/m^3$). The simulated diurnal cycle is lower than the observed one: CHIMERE overestimates the daily minimum and underestimates the maximum. The temporal correlation (R pearson coefficient) varies between 0.53 in daily mean and 0.57 in hourly mean. The spatial distribution of bias and correlation scores of daily maximum values for each summer is shown in SI (Fig. S4). The highest bias ($> +25\mu g/m^3$) and lowest correlations (R of about 0.2) are obtained near large urban areas (e.g. Madrid, Milano) which may be less well represented in the model even if the stations are classified as rural background. There are substantial uncertainties related to the NO_x/VOC emissions in (peri-)urban areas.

These O_3 scores show an overall agreement with those calculated by Gaubert et al. (2014) and Menut et al. (2021) over Europe. The averaged daily maximum bias and correlation coefficients computed are slightly higher and lower, respectively, in this study mainly because the area is limited to Southwestern Europe. Due to the multiple sources of O_3 precursors and favorable temperature and light conditions, the Mediterranean is identified as a region of important uncertainty for modelling O_3 concentration (Richards et al., 2013).

Validation scores are also computed for the surface NO_2 using the EEA observations, with a different distribution of stations that for O_3. In agreement with the results of Menut et al. (2021), CHIMERE underestimates NO_2 concentrations (+4.95$\mu g/m^3$ in daily mean and +8.57$\mu g/m^3$ in daily maximum) compared to EEA observations. Interference from other oxidized nitrogen species in the chemiluminescence analyzer (e.g. Lamsal et al., 2008) may explain the constant underestimation compared to observations. The mean temporal correlation coefficients do not exceed 0.4. These low validation scores may also be linked to the emission inventory used as well as meteorological conditions (boundary layer height representation in particular). As a major O_3 precursor, part of the uncertainty of this study is directly related to NO_2 emissions and concentrations.

Finally, as a critical variable for simulating diurnal and seasonal O_3 concentrations, T_{2m} values have been compared to the E-OBS observations. Averaged over the Southwestern Europe, the bias is close to $0°C$ while the RMSE is significant (8.19$°C$ in daily mean and 12.63$°C$ in daily maximum). The spatial distribution of the bias presents large variations (SI: Fig. S5). The daily maximum T_{2m} is overestimated in the Southern Mediterranean (up to $5°C$) compared to observations while it is underestimated in the northern part (up to $5°C$). Nevertheless, the averaged scores of temporal correlation are high (around 0.75). Even if such validation scores are close to those found in the scientific literature (e.g. Panthou et al., 2018), the temperature uncertainties significantly contribute to those of the O_3 simulated by CHIMERE.

5 Results

5.1 Sensitivity to soil dryness and biomass decrease effects

The sensitivity analysis to soil dryness and biomass decrease effects is focused on summer 2012 as droughts mainly occurred during this year (over the 2012-2014 period). Most of Southwestern Europe was affected by a biomass decrease in 2012 (compared to the wet summer 2014), except Eastern Spain. The LAI difference between summer 2012 and 2014 can reach -30% over central Italy (Appenines region) corresponding to a mean decrease of 0.5 m^2/m^2 (SI: Fig. S3).

C_5H_8 is the main contributor to the total mass of $BVOCs$ emitted (70%) in our study area, followed by the model species APINEN (13%, including e.g. α-pinene, sabinene).

5.1.1 C_5H_8 emissions

Figure 2~~(lower panel)~~ a shows the daily mean C_5H_8 emissions in Southwestern Europe for summer 2012 simulated by the MEGAN model ("Reference" simulation). The spatial distribution of C_5H_8 over the Mediterranean is heterogeneous, ranging from areas of zero or low emissions ($\sim 1 \times 10^{-3} g.m^{-2}.h^{-1}$) to high emitting areas ($\sim 1.5 \times 10^{-3} g.m^{-2}.h^{-1}$) such as in the

Table 2. Comparisons between observed and simulated surface O_3 concentration, NO_2 concentration and 2m temperature, averaged over Southwestern Europe during summer 2012, for the "Reference" CHIMERE simulation.

	Observations	Model	Bias (obs. - mod.)	RMSE	Pearson correl. (R)
O_3	$[\mu g/m^3]$	$[\mu g/m^3]$	$[\mu g/m^3]$	$[\mu g/m^3]$	
Hourly	83.21	85.14	-1.93	20.45	0.57
Daily mean	83.93	84.06	-0.13	14.31	0.53
Daily max	116.32	105.39	10.94	21.49	0.54
NO_2	$[\mu g/m^3]$	$[\mu g/m^3]$	$[\mu g/m^3]$	$[\mu g/m^3]$	
Hourly	7.65	3.70	3.95	5.57	0.25
Daily mean	7.55	2.60	4.95	5.24	0.40
Daily max	14.65	6.08	8.57	9.87	0.37
T_{2m}	$[°C]$	$[°C]$	$[°C]$	$[°C]$	
Daily mean	22.25	22.25	-0.01	8.19	0.76
Daily max	23.13	28.34	0.56	12.63	0.75

400   Balkans, Apennins, Sierra Morena, Sardinia and Central Portugal. Similar spatial distributions were found for APINEN model species. Differences in spatial patterns among species depend on the variation of emission factors over the land cover classes. The effect of biomass decrease and soil dryness on C_5H_8 emissions during the dry summer 2012 is also shown in Figure 2. Biomass decrease averaged over June, July and August is characterized by negative differences of emissions over most of the southern part of the region, reaching -20% in Northern Spain and -25% in Northern Italy.

405   The impact of soil dryness is assessed with the "γ_{SM}-emiss", "γ_{SWS}-emiss" and "γ_{SWSfit}-emiss" MEGAN simulations. The quantified impact can vary considerably between them. In the "γ_{SM}-emiss" experience, C_5H_8 emissions stay constant as long as the soil moisture is above the wilting point (θ_w). Once this point is reached (water is missing), it is assumed that plant can not synthesize C_5H_8 anymore and the emissions decrease steeply. θ_w is constant and depends only on the soil type. For instance, silt soil is characterized by lower θ_w than clay soil, so that soil dryness is more quickly reached for the latter. Due to

410   the high spatial variability of soil type, the difference induced by "γ_{SM}-emiss" is also characterized by large variability. Within a same region (e.g. Central Italy), the difference sharply varies between -50% and 0% while the region is all over affected by an agricultural drought according to the PLA_{SD} indicator (SI: Fig. S2).

For the alternative approach based on the dynamical SWS function, the relative difference of C_5H_8 emissions ("Reference" .vs. "γ_{SWS}-emiss" experiment) is more spatially homogeneous than "γ_{SM}-emiss", and the overall reduction is larger. The

415   strongest stress values are located in plains and for plants with short-root systems, in agreement with the sensitivity analysis performed by Vicente-Serrano (2007) about drought effects on vegetation. Semi-arid regions (e.g. Andalusia) are strongly affected as the water budget is almost permanently in deficit (high solar radiation and low/no precipitation). Being adapted to

recurrent droughts, some plant species (e.g. *Arundo donax* in a Moroccan ecotype) can reduce the C_5H_8 synthesis as the result of pressure selection to preserve their viability (Haworth et al., 2017). However, the emission reduction could be overestimated

420 as irrigation is largely used in many semi-arid areas (e.g. García-Vila et al., 2008). A specific analysis should be undertaken to cover the diversity of responses to drought stress in both natural and human influenced systems within such regions.

The third experiment "γ_{SWSfit}-emiss" presents the same areas of C_5H_8 decrease as "γ_{SWS}-emiss" but in a lower extent. C_5H_8 emissions decrease when SWS values are the lowest. Semi-arid regions are also more affected (-50%) than others (e.g. -20% in Central Italy).

425 Three areas of high emissions are analyzed more specifically (boxes in Fig. 2): the Balkans, the Pô Valley and Central Spain. Their temporal evolution of C_5H_8 emissions during the summer 2012 for the different experiments are shown in Figure 3. Droughts and heatwaves occured over the three regions. Droughts do not negate the dependence on light and/or temperature, and emission peaks are driven by heatwaves with higher 2m temperature and solar radiation (SI: Fig. S6). However, the peak values are reduced if LAI decrease and soil dryness are accounted for. Averaged over the three regions, the biomass decrease

430 induces a 3% decrease of the total summer amount of C_5H_8 emitted. The soil dryness parameter induces difference of -12% for "γ_{SM}-emiss", -39% for "γ_{SWS}-emiss" and -13% for "γ_{SWSfit}-emiss". Based on experimental measurements over three summers (2012, 2013 and 2014) in a Mediterranean environment (Observatoire de Haute Provence, *Quercus pubescens* plant species), Saunier et al. (2017) identified a 35% emission decrease due to severe droughts. Demetillo et al. (2019) measured in California a C_5H_8 concentration reduction of 50% during severe droughts (2014 and 2015). These values are close to and even

435 above the range of the simulated experiments. "γ_{SWS}-emiss" experiment is considered here as the upper limit of the reduction range of C_5H_8 emissions due to dry conditions, SWS being included in the calculation of the emissions rate as soon as soil water stress for plant stress is below 0.5.

In addition, the different simulated experiments from the MEGAN-CHIMERE model have been compared to observations of surface C_5H_8 concentrations from EBAS data set (Fig. 4). The Ersa station having an almost complete time series for

440 summer 2012, is kept. Based on the PLA indicator, Northern Corsica was affected by two heatwaves but no drought. However, we detected soil dryness conditions close to the drought limit (mean PLA_{SD} of -0.09). The temporal correlation between simulated and observed C_5H_8 concentrations is similar for each experiment (R coefficient around 0.68). Averaged over the summer, the lowest mean bias with the observations is obtained with "γ_{SWSfit}-emiss" (-28 pmol/mol) and the largest one with "γ_{SM}-emiss" (-151 pmol/mol). Over July and August, "γ_{SWS}-emiss" experiment presents the lowest mean bias (+56

445 pmol/mol). The "Reference" and "γ_{SM}-emiss" experiments have equal values as the soil wetness from WRF-Noah is above the local wilting point. However, this comparison with observations is made at a single station. It would be valuable to carry out the same exercise at several locations (including areas representative of semi-arid environment) and over several summers. Finally, biogenic emission models (such as MEGAN) consider in general a reduction in emissions when drought episodes occur only for isoprene (C_5H_8). However, there is a lot of uncertainty on how plant activity reacts to water stress. In the

450 case of C_5H_8 species, the response to water stress could occur in two phases: a state of increasing emissions due to leaf temperature stimulation during the drought onset, followed by a state of C_5H_8 synthase limitation (Potosnak et al., 2014). For monoterpenes, the response to water stress may be different depending on the species (Bonn et al., 2019). For instance,
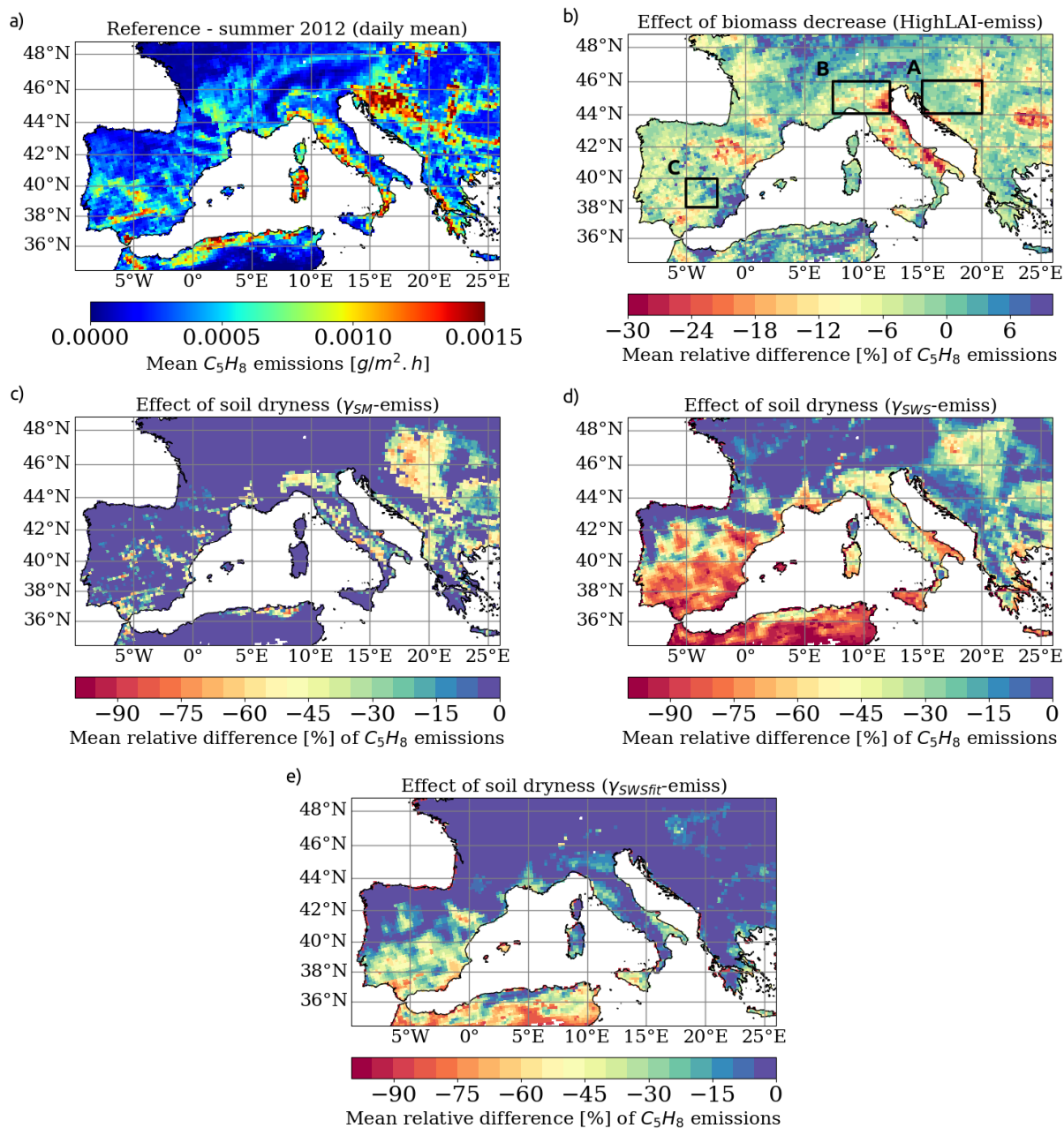
Figure 2. Summer mean (JJA) of daily mean C_5H_8 emissions $[g.m^{-2}.h^{-1}]$ for 2012 from the "Reference" simulation (~~lower panel~~a). Mean relative difference [%] of C_5H_8 emissions due to biomass decrease and soil dryness. The relative difference is computed between the "Reference" and "HighLAI-emiss" simulation to quantify the biomass decrease effect (~~upper left panel~~b), and "γ_{SM}-emiss" (c) / "γ_{SWS}-emiss" (d) / "γ_{SWSfit}-emiss" (e) to quantify the soil dryness effect. For diagnostic purposes, areas of interest are designated within the dashed rectangles: here named as the "Balkans" (A), "Pô Valley" (B) and "Central Spain" (C).
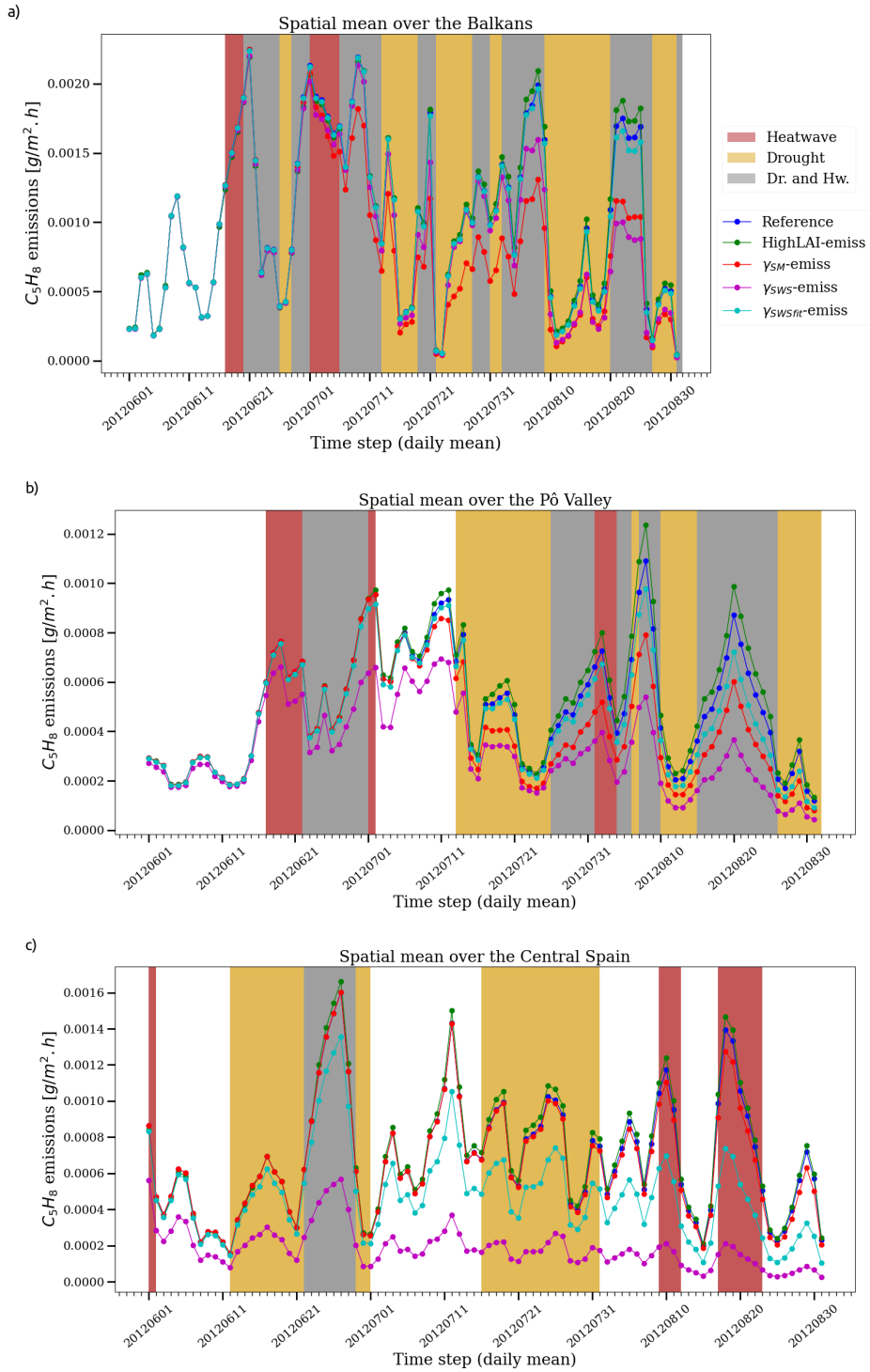
Figure 3. Daily mean C_5H_8 emissions $[g.m^{-2}.h^{-1}]$ during the summer 2012, spatially averaged over the Balkans (~~upper panel~~a), Pô Valley (~~middle panel~~b) and Central Spain (~~lower panel~~c) for the different MEGAN experiments. The colored bands highlight periods of droughts and heatwaves.
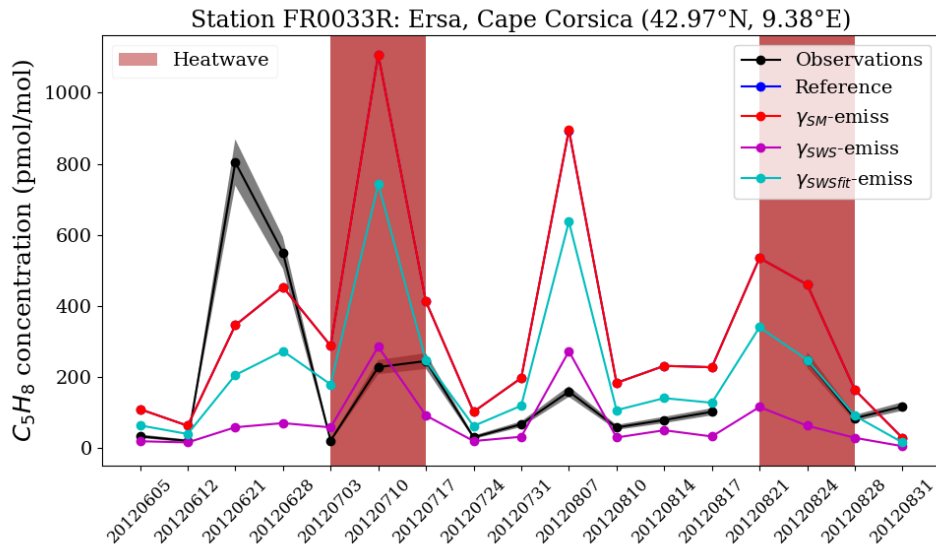
Figure 4. Observed surface C_5H_8 concentration [$pmol/mol$] during the summer 2012 at the Ersa station (FR0033R, Cape Corsica) from the EBAS data set, compared to the different simulated experiments undertaken by the MEGAN-CHIMERE model. The shaded curve in black represents the precision range of the measurements. The "Reference" and "γ_{SM}-emiss" experiments here have equal values. Maximum PLA_{T2m} and PLA_{SD} are +3.2°C and -0.02 of soil dryness index respectively.

sabinene emissions (experimentally measured) from the European beech (*Fagus sylvatica*) decrease strongly with decreasing soil water availability while trans-β-ocimene emissions (from the same plant species) remain constant.

5.1.2 O_3 dry depositon velocity

Figure 5~~(upper left panel)~~ a presents the daily mean dry deposition velocity ranging from 1.0 to 1.8cm/s within our areas of interest. The mean effect of biomass decrease (relative difference between the "Reference" and the "LAIdecr-dep" experiment, ~~upper right panel~~Fig. 5b) over summer 2012 does not exceed -8%, and is lower over the forested areas (as it was prescribed in our experiment).

The cumulative effects of biomass decrease and soil dryness are included in the "LAIdecr-dep/f_{SWS}-dep" experiment (Fig. 5, ~~lower pannel~~c). The soil dryness effect is much larger than that of biomass decrease. Values range from 0 to -35%. Central Italy and the Iberian Peninsula are the most affected regions.

The temporal evolution of O_3 dry deposition velocity for the three areas of interest is shown in Figure 6. The biomass decrease effect is larger (e.g. -9% over the Pô Valley) during the first half of summer. It is close to -1% at the end of summer. This is explained by the LAI decrease prescribed from mid-July in the dry deposition scheme. In addition to that, the dry deposition velocity is characterized by a decreasing trend over summer imposed by the fixed phenology factor (f_{phen}).

Regarding the soil dryness, its effect is almost constant during summer (e.g. -12% over the Pô Valley). Based on measure-
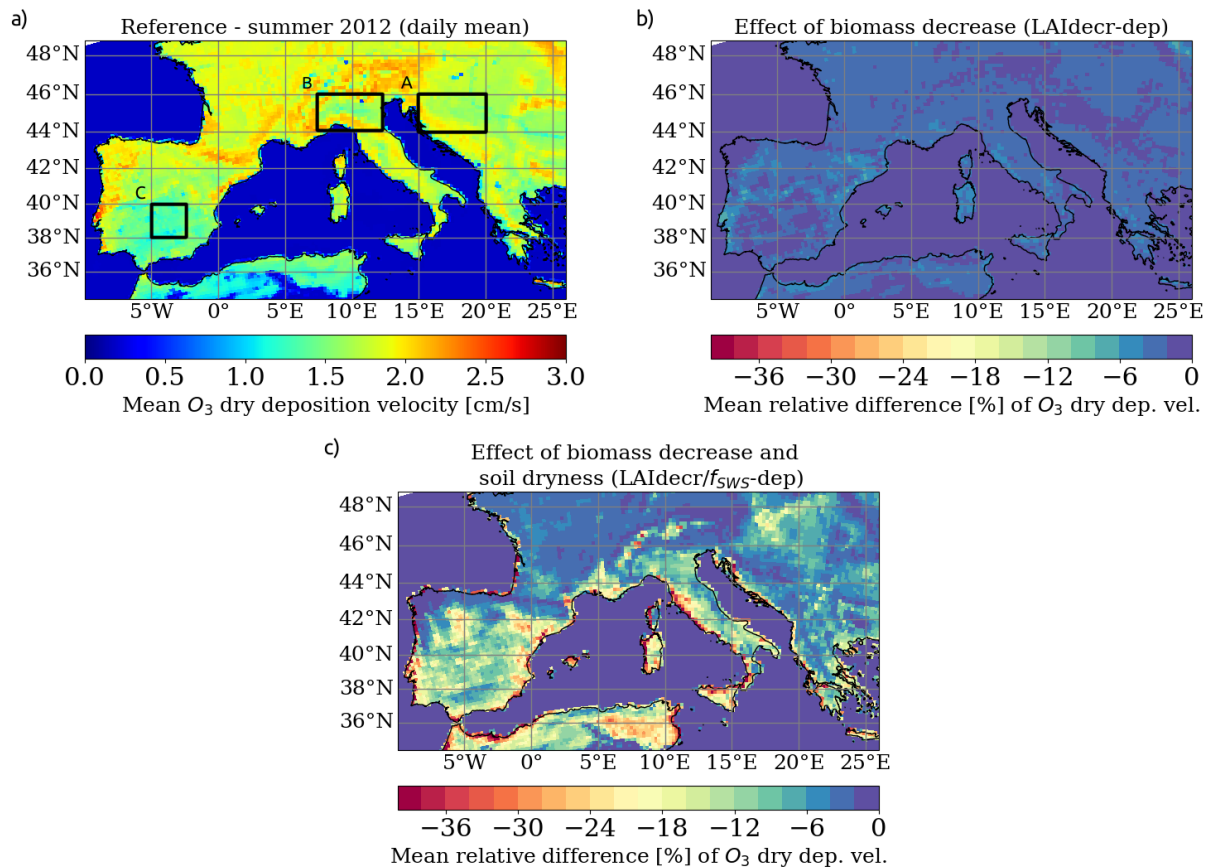
Figure 5. Summer mean (JJA) of daily mean O_3 dry deposition velocity [cm/s] for 2012 from the "Reference" simulation (~~upper left panel~~a). Mean relative difference [%] of O_3 dry deposition velocity due to biomass decrease and soil dryness. The relative difference is computed between the "Reference" and "LAIdecr-dep" simulation to quantify the biomass decrease effect (~~upper right panel~~b) and "LAIdecr-dep/f_{SWS}-dep" to quantify combined biomass decrease and soil dryness effect (~~lower panel~~c).

ments over Central Italy, Lin et al. (2020) computed a relative difference of about -50% between August 2004 (wet summer, ∼0.8cm/s) and August 2003 (dry summer, ∼0.4cm/s). However, summer 2003 was characterized by considerable heatwaves in
470   Italy (positive PLA_{T2m}) which might intensify the decrease. We emphasize that dry deposition velocity generally decreases during heatwaves (Fig. 6) as the near surface temperature is above the optimal temperature of stomatal conductance. Both effects related to droughts and (the most intense) heatwaves lead to a reduction in O_3 deposition. The sensitivity of dry deposition velocity to soil moisture can be considerably different from one deposition scheme to another. Using the same deposition scheme as in the present study, Anav et al. (2018) calculated an average decrease of 10% over Europe in dry O_3 deposition.
475   To the best of our knowledge, there is no study yet in the scientific literature that fully assess the O_3 dry deposition of CHIMERE against observations or its sensitivity to different meteorological forcings. Therefore, we have compared our re-

sults to the measured data available for summer 2012 at the Castelporziano station from the European Fluxex Database (Fig. 6). Based on the PLA indicator, the Lazio region was affected by a severe drought all along the summer (mean PLA_{SD} of +0.05). All simulated experiments overestimate O_3 deposition compared to observations. The "LAIdecr-dep/f_{SWS}-dep" experiment

480 has the smallest average bias (-0.19e-6 g/cm^2) and the highest correlation (R coefficient of 0.40). Such overestimation has also been calculated for models whose ~~gaz~~ gas deposition scheme is based on Wesely (1989) "big leaf" parameterization (e.g. Michou et al., 2005; Huang et al., 2022). As the canopy conductance increases proportionally with the prescribed LAI (Emberson et al., 2000), this could be explained by an overestimation of the LAI that is almost two times larger than the mean LAI reconstructed from MODIS over this area. The importance of representing processes dynamically (as opposed to fixed

485 parameters, especially for the non-stomatal conductance) is also highlighted in order to better simulate the diurnal deposition cycle, and so the daily average values (Huang et al., 2022).

Finally, identifying soil dryness as a major driver of inter-annual variability of O_3 deposition velocity, Lin et al. (2019) emphasize that error in modelling the deposition may considerably rely on the ability of models to simulate accurately the precipitation distribution. They assessed the sensitivity of their deposition velocity scheme (Geophysical Fluid Dynamics Laboratory

490 LM3.0/LM4.0) to two different meteorological forcings and found a factor two over the Northern Europe.

5.1.3 O_3 surface concentration

Figure 8 ~~(upper left panel)~~ a maps the mean surface O_3 concentration simulated by CHIMERE ("Reference" experiment) over the summer 2012. High concentrations (between 100 and $110\mu g/m^3$) are located in the eastern part of the study area (e.g. the Balkans and Italy). The spatial distribution of mean surface O_3 shows similar patterns as the distribution of PLA_{T2m}

495 (SI: Fig. S2), highlighting the critical role of the temperature. Surface O_3 remains high above the sea due to transport and the absence of deposition in the canopy (e.g. $120\mu g/m^3$ over the Adriatic sea). The contribution of BVOC emissions on surface O_3 is also presented (~~upper right panel~~Fig. 8b). BVOC emissions are known to be significant precursors of O_3 production in the Mediterranean region. It varies between 4% (e.g. Iberian Peninsula) and 22% (e.g. Northern Italy) in our study, that is included in the range of values reported in the scientific literature (e.g. Mertens et al., 2020). Finally, our areas of interest are

500 located in rural regions, mostly characterized by a low-NO_x regime (SI: Fig. S7).

A simulation including drought effects on both C_5H_8 emissions and O_3 dry deposition has been conducted with MEGAN-CHIMERE ("γ_{SWS}-emiss & LAIdecr/f_{SWS}-dep" experiment). The resulting effect on surface O_3 is shown in Figure 8 ~~(lower panels)~~. On average during the summer (Fig. 8~~, lower left panel~~c), O_3 concentration is slightly higher over the continent (between +0.5% and +3.0%) due to the decrease of O_3 deposition as dominant effect, while it is slightly lower (between -1%

505 and -1.5%) over the sea and ocean due to the lower transport of O_3 precursors, compared to the "Reference" experiment. However, the O_3 increase over the Iberian Peninsula may be overestimated as the LAI reduction we applied to the whole domain (e.g. -20% for grass PFTs) is larger compared to the variation of MODIS LAI in this specific region (SI: Fig. S3).

Drought effects on surface O_3 induced by C_5H_8 emission reduction is not constant. It is largest during combined heatwaves (i.e. when biogenic contribution is high). As a result, drought effects on C_5H_8 emissions can be dominant (compared to the effects on O_3 deposition) during simultaneous droughts and heatwaves, inducing a decrease of O_3 peaks by a few $\mu g/m^3$ both

510
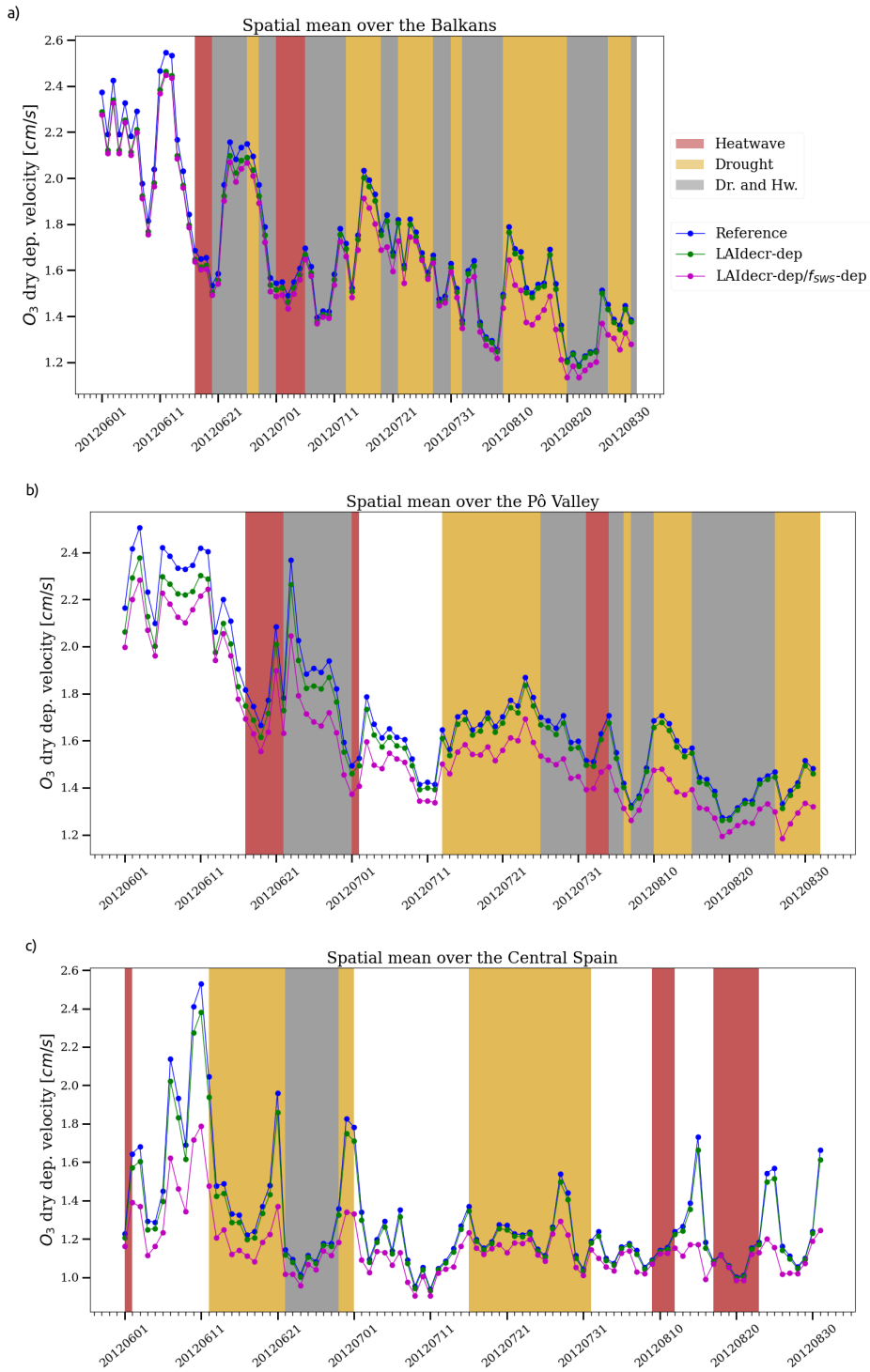
Figure 6. Daily mean O_3 dry deposition velocity [cm/s] during the summer 2012, spatially averaged over the Balkans (~~upper panel~~a), Pô Valley (~~middle panel~~b) and Central Spain (~~lower panel~~c) for the different CHIMERE experiments.
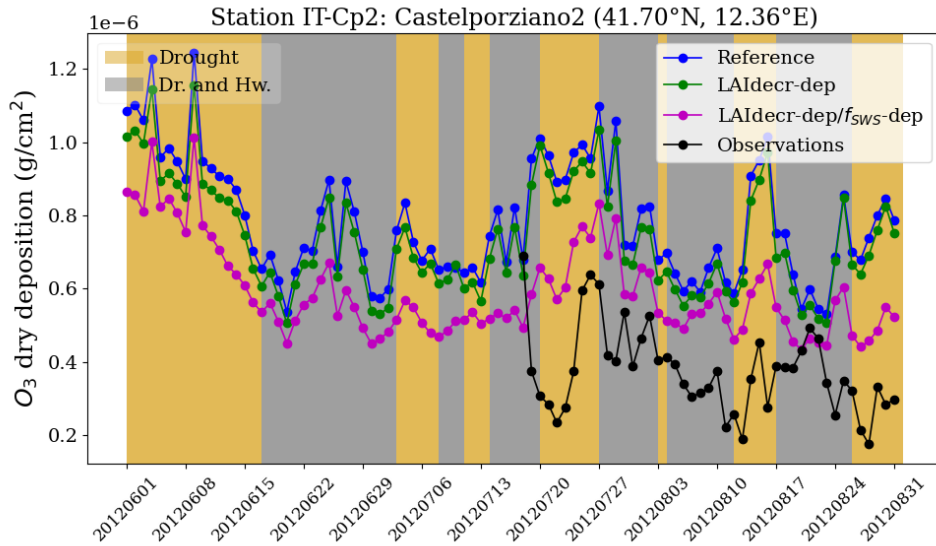
Figure 7. Observed O_3 deposition flux [g/cm^2] during the summer 2012 at the Castelporziano station (IT-Cp2, Lazio region) from the EFDC database, compared to the different simulated experiments undertaken by the CHIMERE model. Maximum PLA_{T2m} and PLA_{SD} are +3.88°C and +0.09 of soil dryness index respectively.

over continent and sea/ocean. The maximum absolute relative difference (Fig. 8, ~~lower right panel~~d) reaches -5% over the Pô Valley and -14% along the Strait of Gibraltar. O_3 formation over the latter is favoured by large NO_x shipping emissions. Conducting a similar modelling experiment based on the γ_{SM} from MEGANv3, Jiang et al. (2018) simulated a maximum absolute relative difference of surface O_3 of about -4% in August 2010. O_3 reduction (-10% on average) due to severe droughts

515   was also measured in California over the period 2002-2015 (Demetillo et al., 2019). This was identified as being related to a steep decrease of C_5H_8 concentrations.

For each area of interest, the temporal evolution of surface O_3 based on the different CHIMERE experiments and the EEA observations (AQ e-Reporting) is presented (Fig. 9 for the Pô Valley and Fig. S8 for the Balkans and Central Spain in SI). Since the resulting effects of biomass decrease and soil dryness on surface O_3 are less than the bias between model and observations

520   in our study (see Sect. 4), no simulation can be designated with certainty as the best fit.

5.2   Statistical variation during droughts and heatwaves

In this result section, a statistical analysis is performed using ~~observations and simulations of the summers 2012, 2013 and 2014.~~ CHIMERE simulations and several observational data sets. The "all-emiss-dep" experiment has been chosen for simulating

525   summers 2012-2014 because it includes drought and heatwave effects in the most comprehensive way. Moreover, the C_5H_8 emission approach "γ_{SWSfit}-emiss" has shown good performance compared to observations (Fig. 4), remaining rather con-
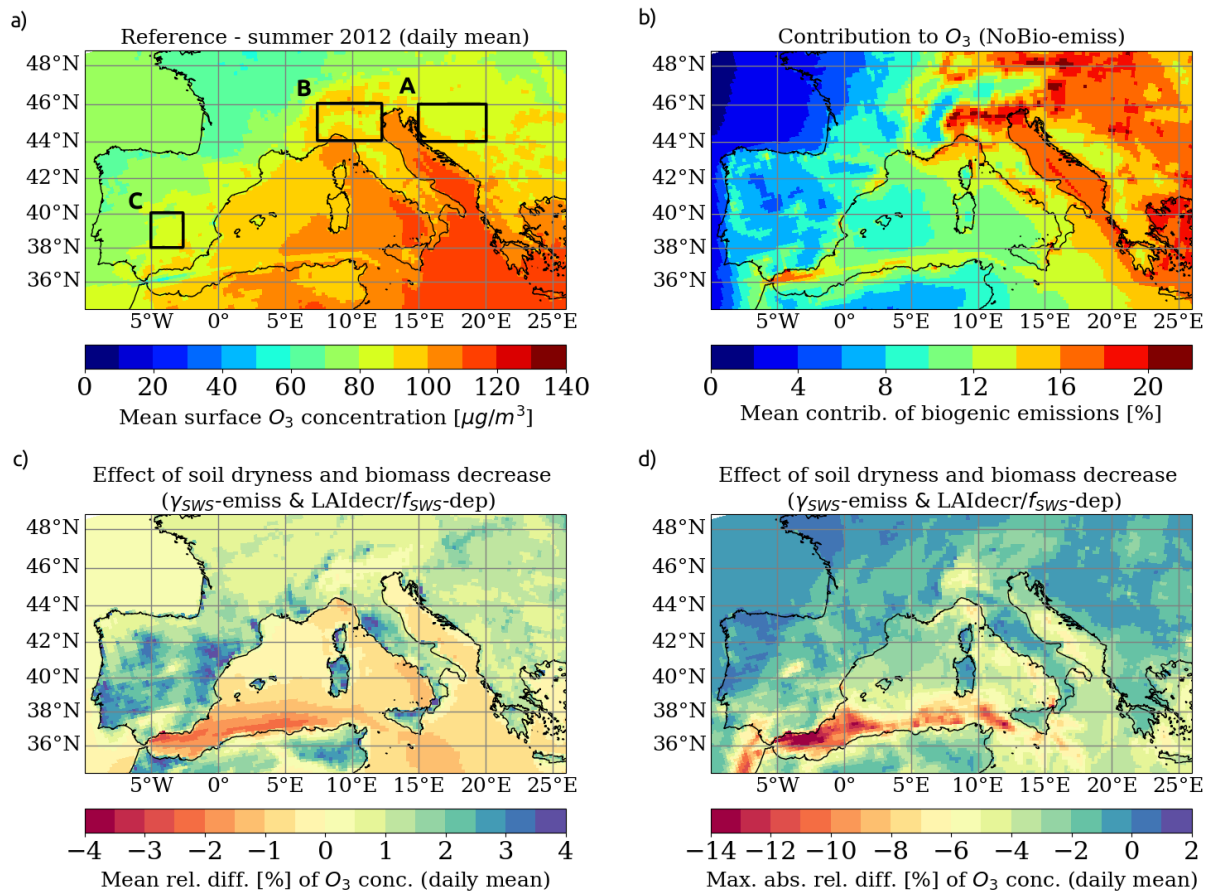
Figure 8. Summer mean (JJA) of daily mean O_3 surface concentration $[\mu g/m^3]$ for 2012 from the "Reference" simulation (~~upper left panel~~a). Mean contribution of biogenic emissions to O_3 surface concentration based on the "NoBio-emiss" experiment (~~upper right panel~~b). Mean (~~lower left panel~~c) and maximum absolute (~~lower right~~d) relative difference [%] of O_3 surface concentration due to biomass decrease and soil dryness. The relative difference is computed between the "Reference" and "γ_{SWS}-emiss & LAIdecr-dep/f_{SWS}-dep" simulation from CHIMERE.
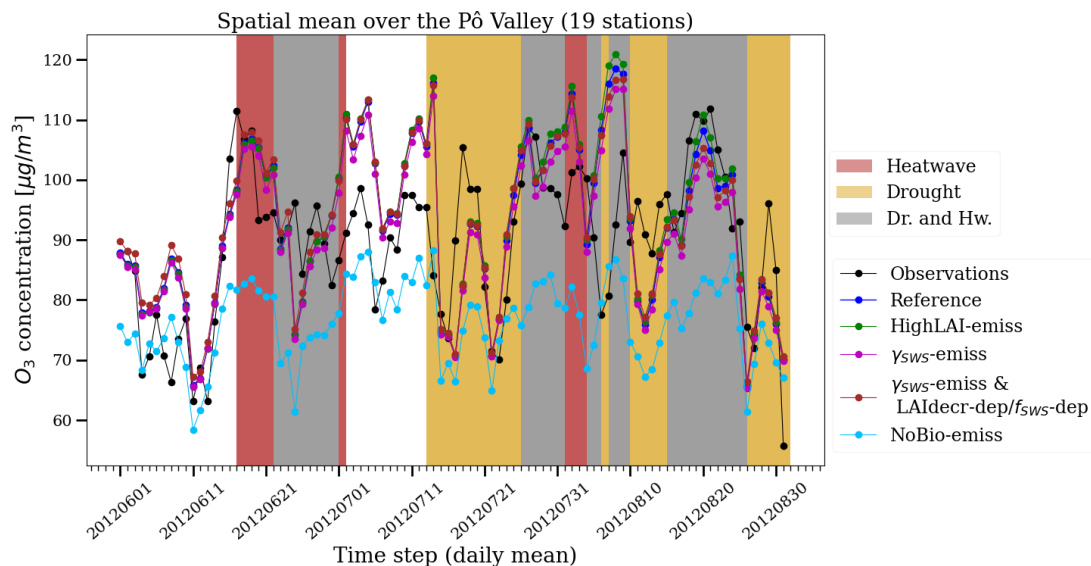
Figure 9. Daily mean O_3 surface concentration [$\mu g/m^3$] during summer 2012, spatially averaged over the Pô Valley from the EEA observations and the different CHIMERE experiments.

servative, not in the higher limit of the C_5H_8 reduction range.

Clusters of droughts and heatwaves (isolated or combined) are constructed based on the PLA_{T2m} and PLA_{SD} indicators, allowing to analyze the statistical variation of simulated C_5H_8 emissions, O_3 stomatal conductance and O_3 surface concentration

530 ~~(both from observations and simulations)~~ for summers 2012-2014. We performed the same analysis on observations of $HCHO$ total column for summers 2005-2016 and O_3 for summers 2000-2016. Using those indicators, the following conditions were defined and grouped into clusters: "heatwaves or droughts", "heatwaves and droughts", "heatwaves and not droughts" and "droughts and not heatwaves". Normal conditions are defined as no drought and no heatwave.

5.2.1 C_5H_8 emissions

535 Figure 10 shows the distribution of C_5H_8 emission rates over the Southwestern Mediterranean for clusters of extreme weather events. On average, the daily maximum C_5H_8 emission is significantly higher (t-test, p < 0.01) during isolated and combined heatwaves than normal conditions (no heatwave nor drought) with a mean value of 0.16×10^{-2} against $0.12 \times 10^{-2} g.m^{-2}.h^{-1}$. However, emissions during droughts have the same mean value as in normal conditions. During isolated droughts (cluster "drought and not heatwave"), the mean daily maximum C_5H_8 emission rate is lower than normal conditions ($-0.02 \times$

540 $10^{-2} g.m^{-2}.h^{-1}$, non-significant difference). These results are in general agreement with the observed $HCHO$ total column by satellite instrument, used as proxy of BVOC emissions variation (see Sect. 5.2.2).

Weather conditions are considerably different between droughts combined with heatwaves and those which are not (SI: Fig. S9).
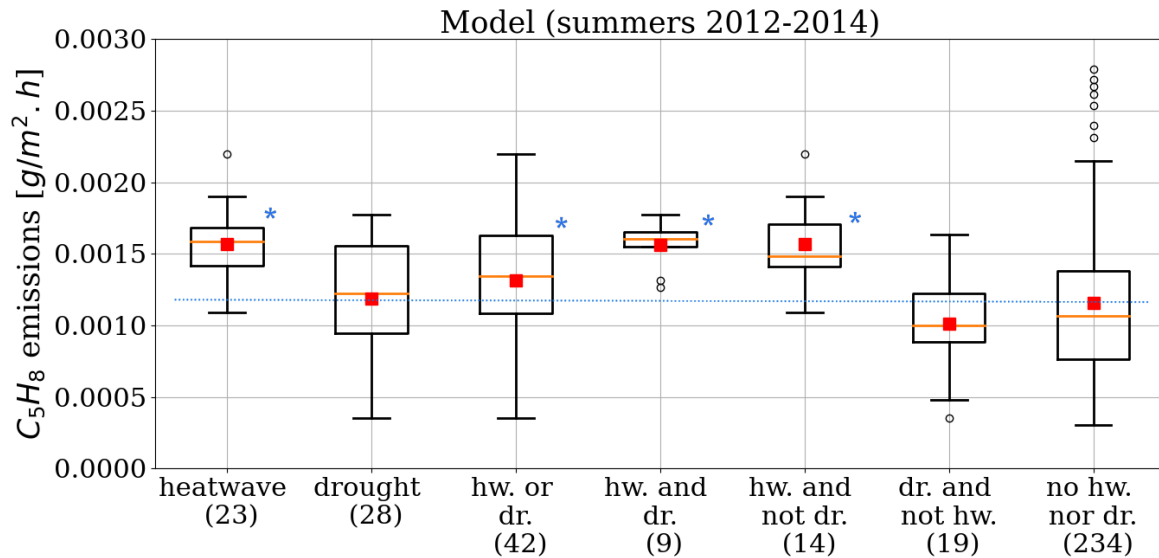
Figure 10. Daily maximum C_5H_8 emission rate $[g.m^{-2}.h^{-1}]$ simulated by the MEGAN model ("γ_{SWSfit}-emiss" experiment) over Southwestern Europe, clustered by identified extreme weather events (PLA_{T2m} and PLA_{SD} indicators from RegIPSL). The number of days is indicated in parentheses. The analyzed period is June-July-August 2012, 2013 and 2014, covering a total of 276 days. The red squares show the mean of the distribution and the black circles are the outliers. The blue dotted line indicates the mean value of the normal conditions ("no hw. nor dr." cluster) and the blue stars if the mean value of the considered cluster is significantly different (t-test, at least p < 0.1) from the normal conditions. The box covers the InterQuartile Range (IQR) between Q1 (25th percentile) and Q3 (75th percentile). The lower whisker is limited to a statistical minimum (Q1-1.5*IQR) and the upper one to a statistical maximum (Q3+1.5*IQR).

The combined (resp. isolated) droughts are characterized by a 2m temperature of 23.9°C (resp. 22.6°C), a shortwave radiation of 342.2W/m^2 (resp. 296.0W/m^2) and a cloud cover of 1.8% (resp. 3.1%). Those weather variables are used for the computation of the activity factors γ_P and γ_T, thus directly affecting emissions. During isolated droughts, γ_{LAI} (0.48) and γ_{SWS} (0.76) are smaller than for normal conditions (0.51 and 0.89 respectively, significant difference for both). Nevertheless, this negative signal is not large enough for significant variation of the emission rates (compared to normal conditions).

Gathering worldwide data from experimental measurements of biogenic emissions under different climate drivers, the scientific review presented by Feng et al. (2019) (based on 74 articles) estimated to +53% the emission change of C_5H_8 during warm conditions and -15% during dry conditions. Those variations are close to what we simulated (+35% and -13% respectively).

5.2.2 $HCHO$ total column

$HCHO$ is a product of oxdation of VOCs. Based on the "Reference" and "NoBio-emiss" CHIMERE simulations, we computed that biogenic emissions contribute between 60 and 80% of the $HCHO$ concentration over Southwestern Europe. Variations of $HCHO$ concentration may therefore be used as indicator of BVOC emission variations during droughts and heatwaves. This

allows us to use satellite observations of $HCHO$, which is particularly interesting due to the lack of in-situ data. Observations of the $HCHO$ total column from the OMI instrument are used.

Table 3 presents the average difference of $HCHO$ ($\Delta HCHO$) during extreme events compared to normal conditions (no heatwave nor drought), based on the OMHCHOd product. Over summers 2005 to 2016, $HCHO$ is significantly higher during heatwaves for the Balkans, Pô Valley and Central Spain (+15% on average). $\Delta HCHO$ is also positive during droughts but to a lesser extent (+3% on average, non-significant for Central Spain only). However, isolated droughts induce a significant decrease for the Balkans (-7%), Pô Valley (-6%) and Central Spain (-6%). Those results are consistent with the variation of C_5H_8 emissions simulated by MEGAN when a soil moisture parameter is considered (see Sect. 5.2.1). Wang et al. (2021a) also report a significant $HCHO$ column decrease (up to -30%) induced by a prolonged drought in a forested area in China.

The observed and simulated $HCHO$ total columns have been compared for the "γ_{SWSfit}-emiss" experiment over summer 2012. Time series showing $HCHO$ evolution for the three areas of interest are shown in SI (Fig. S11). Simulated $HCHO$ columns are generally higher than those from observations, especially for the Balkans. As mentioned in Sect. 2.2, uncertainty on the observations is large (between 30 and 100%) with large spatial variability (about a factor of two larger than in CHIMERE). HCHO products from OMI also present high uncertainty and in particular a systematic low mean bias (20-51%) (Zhu et al., 2016).

$HCHO$ differences could be due to wrong specifications of land cover, and thus of the EF of C_5H_8 (e.g. Curci et al., 2010). Temperate tree PFTs are characterized by high C_5H_8 emission rates (respectively 10 000 and $600\mu g.m^{-2}.h^{-1}$ for broadleaf and needleleaf types), compared to grassland ($800\mu g.m^{-2}.h^{-1}$) or cropland ($1\mu g.m^{-2}.h^{-1}$) (Guenther et al., 2012). After aggregation of the USGS land cover classes, the vegetation type assumed in CHIMERE in the Balkans, for instance, is 57% of forest cover, 9% grassland and 33% cropland. Using the MODIS MCD12 product (Friedl et al., 2010), we find a different distribution, with 30% of forest cover, 25% grassland and 31% cropland (SI: Fig. S10). The choice as well as the temporal evolution of the land cover database are crucial for the calculation of C_5H_8 emissions (Chen et al., 2018). Despite the use of satellite data for land cover, significant uncertainties remain in the calculation of C_5H_8 emissions due to the classification of vegetation types and species (Opacka et al., 2021).

The comparison of $HCHO$ total column variations for CHIMERE and OMI during droughts and heatwaves relies on a limited number of cases. It is therefore difficult to support conclusions with a sufficient level of certainty. Nevertheless, results suggest that CHIMERE simulations are more sensitive to temperature than the OMHCHOd OMI observations (+52% and +28% during heatwaves respectively, averaged over the three areas of interests). Since the summer 2012 was affected by long agricultural droughts, the inclusion of a soil dryness parameter in CHIMERE ("γ_{SWSfit}-emiss" experiment) reduces the simulated $HCHO$ peaks (SI: Fig. S11). However, the mean simulated $\Delta HCHO$ during heatwaves and droughts is similar in the "γ_{SWSfit}-emiss" and "Reference" experiments (decrease of -2% and -1% respectively). The temporal correlation does not vary significantly either (e.g. R coefficient around 0.5 for the Balkans).

Finally, the observed variations of total $HCHO$ over summers 2005-2006 and the three areas considered here were also computed with OMI-BIRA retrieval. During heatwaves, both show a significant increase: +31% for OMI-BIRA (and +15% for OMHCHOd). The increase is lower during droughts: +13% (and +3%). The variation becomes slightly negative during

Table 3. Variation of HCHO total atmospheric column [$molecules/cm^2$] (ΔHCHO) due to heatwaves, droughts and isolated droughts in comparison to normal conditions (no heatwaves nor droughts) for summers (JJA) between 2005-2016 (measurements at 1pm). Summer 2012 is compared with CHIMERE simulations. Results are computed for each pixels and averaged over areas of interests: the Balkans, Central Italy and Central Spain. Stars mean that the difference with normal conditions is statistically significant (t-test, p < 0.1).

	OMI (2005-16)	OMI (2012)	CHIMERE (2012)	
			Reference	γ_{SWSfit}-emiss
Balkans (norm. cdt.)	5.7×10^{14} $mol./cm^2$	4.0×10^{14} $mol./cm^2$	7.6×10^{14} $mol./cm^2$	7.6×10^{14} $mol./cm^2$
Δ with heatwaves	+ 17 %*	+ 64 %*	+ 94 %*	+ 92 %*
Δ with droughts	+ 6 %*	+ 54 %*	+ 63 %*	+ 62 %*
Δ with isolated droughts	- 7 %*	+ 32 %*	+ 10 %*	+ 9 %*
Pô Valley (norm. cdt.)	5.9×10^{14} $mol./cm^2$	5.3×10^{14} $mol./cm^2$	7.6×10^{14} $mol./cm^2$	7.5×10^{14} $mol./cm^2$
Δ with heatwaves	+ 16 %*	+ 17 %*	+ 36 %*	+ 34 %*
Δ with droughts	+ 2 %*	+ 11 %*	+ 24 %*	+ 23 %*
Δ with isolated droughts	- 6 %*	- 1 %	- 3 %*	- 3 %*
Central Spain (norm. cdt.)	5.2×10^{14} $mol./cm^2$	4.8×10^{14} $mol./cm^2$	6.1×10^{14} $mol./cm^2$	5.8×10^{14} $mol./cm^2$
Δ with heatwaves	+ 12 %*	+ 2 %	+ 28 %*	+ 25 %*
Δ with droughts	+ 0 %	- 7 %*	+ 9 %*	+ 8 %*
Δ with isolated droughts	- 6 %*	- 11 %*	- 3 %*	- 3 %*

isolated droughts: -2% (and -6%). This comparison highlights the uncertainty in the satellite observations but also that the general behavior is consistent in both retrievals and similar to what was obtained for 2012 using CHIMERE.

5.2.3 O_3 stomatal conductance

Surface weather conditions are critical for the stomatal conductance and therefore influence the dry deposition velocity. Figure 11 shows the maximum daily stomatal conductance of O_3 ("LAIdecr/f_{SWS}-dep" CHIMERE experiment) clustered by simulated extreme weather events and averaged over the Western Mediterranean. The same analysis has been performed on the dry deposition velocity and signals induced by extreme weather events are similar.

Droughts and heatwaves (isolated or combined) induce a significant decrease of the O_3 stomatal conductance, quantified at -25% for heatwaves and -35% for droughts compared to normal conditions. The activity factors mainly affected by droughts and heatwaves are f_{temp}, f_{VPD} and f_{SWS}.

The variation of f_{temp} during heatwaves depends on the magnitude of the events and so on their location, since the percentile of PLA indicator is defined for each grid cell. Over the Pô Valley and Balkans for instance, most heatwaves are characterized
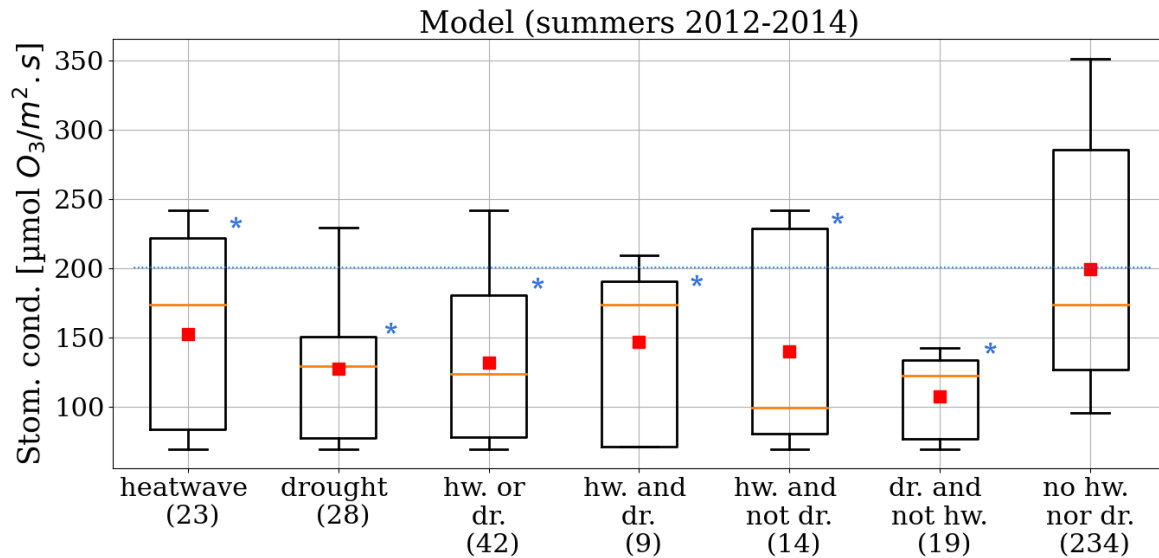
Figure 11. Same as Figure 10 with the simulated O_3 stomatal conductance $[\mu mol O_3.m^{-2}.s^{-1}]$ by the CHIMERE model ("LAIdecr/f_{SWS}-dep" experiment).

by temperatures close to optimal values of stomatal conductance that is fixed around 24°C (SI: Fig. S6). However, for those occurring in Central Spain (between 30° and 32°C), f_{temp} decreases by 7% compared to normal conditions. The temperature limit before complete stomatal closure is set at 40°C. Therefore exceptional heatwaves occurring in Southern Spain for instance

605 could lead quickly to an accumulation of O_3 at the surface. f_{VPD} that depends both on temperature and relative humidity; significantly decreases during droughts and heatwaves (e.g. -6% averaged over the Southwestern Europe). Finally, f_{SWS} is the factor dominating the signal of variation of stomatal conductance. At the Southwestern Europe scale, this factor is the lowest during isolated droughts with a mean decrease of -35%.

5.2.4 O_3 surface concentration

610 Figure 12 shows the distribution of the observed (summers 2000-2016 and 2012-2014) and simulated (summers 2012-2014) daily maximum surface O_3 concentrations over Southwestern Europe for each cluster of extreme events. Observed O_3 (~~upper panel~~Fig. 12a) is significantly (t-test, $p < 0.01$) higher during heatwaves ($+18\mu g/m^3$) and droughts ($+9\mu g/m^3$) than during normal conditions. Considering all droughts over the United States of America, Wang et al. (2017) also computed a mean increase in surface O_3 (+17% compared to the average). During isolated droughts in our study area, daily maximum O_3 is

615 larger ($+4\mu g/m^3$) but the difference is non-significant.

The distribution of the simulated surface O_3 ("all-emiss-dep" experiment) by extreme events over the period 2012-2014 (~~lower panel~~Fig. 12c) presents similar signals but of lower magnitude: $+9\mu g/m^3$ during heatwaves, $+3\mu g/m^3$ during droughts and

non-significant difference during isolated droughts compared to normal conditions. Based on the results discussed above, the difference between the "heatwave" and "isolated drought" cluster could be explained by the different conditions of biogenic

620 emissions, dry deposition, temperature and light. However, observations over the same period (~~middle panel~~Fig. 12b) present a significant increase of the daily maximum O_3 during isolated droughts ($+9\mu g/m^3$), unlike what we simulated. The C_5H_8 emission reduction effect during such extreme event could be counterbalanced in a larger extent by the O_3 dry deposition decrease. It could also be explained by an underestimated impact of the enhanced photochemistry in the simulations, as we simulated favorable weather conditions during both combined and isolated droughts.

625 In summary, the variation of canopy-troposphere interactions (simulated by the MEGAN and CHIMERE models) during droughts and heatwaves is characterized by a consistent signal with respect to O_3 observations (except for the isolated droughts over summers 2012-2014). Meteorological conditions are critical for the O_3 budget especially during summer droughts and heatwaves. In addition to uncertainties in the modelling of precursor emissions and O_3 deposition (as mentioned above), differences between observations and simulations may also rely on meteorological uncertainties, such as the diurnal temperature

630 cycle (see Sect. 4) and the Planetary Boundary Layer Height (PBLH). The night-time representation of the PBLH is often misrepresented in the WRF model (e.g. Chu et al., 2019).

5.3   Threshold level exceedance of O_3

In the European Union, the air quality standard for O_3 exposure is set at a daily maximum concentration of $120\mu g/m^3$ (8h-average) (EEA, 2020). Figure 13 shows the number of days above this threshold based on the AQ e-Reporting observations and

635 the CHIMERE "all-emiss-dep" simulations for summers 2012, 2013 and 2014. Summers 2012 and 2013 present a large number of days exceeding the standard concentration. Even if exceedances occur in similar regions for observations and simulations, the number of days is generally larger in the observations. This is due to the overall underestimated daily maximum in CHIMERE compared to observations (see Sect. 4). For example in the Pô Valley, that is the most affected region in Southwestern Europe, around 60 exceeding days were observed and 50 were simulated over the summer 2012. This region is known for its highly

640 polluted air (O_3 and its precursors) due to high anthropogenic emissions and unfavorable topographic and meteorological conditions for pollutants dispersion (e.g. Bigi et al., 2012). Other regions affected by O_3 peaks can be highlighted: Southeastern France, central Spain and central Italy for both summers 2012 and 2013.

Table 4 presents the distribution characteristics of stations with at least one day above the EU standard during summer period. On average over 2000-2016, that concerns 54% of EEA stations over the Western Mediterranean. The average number of

645 exceedance days per station is 27 (almost a third of the summer period). Summer 2012 is above the 2000-2016 average, with 61% of stations affected and 28 days on average per station. For the same year, co-located values from CHIMERE simulations ("all-emiss-dep" experiment) are lower: 57% of stations and 18 days on average.

Over all summers between 2000 and 2016, 34% of the exceeding days occurred during heatwaves (with a mean exceeding value of $24\mu g/m^3$) and 27% during droughts ($+18\mu g/m^3$). The number of days decreases by 13% if we consider only the

650 isolated droughts (14%, $+15\mu g/m^3$). Summer 2012 was affected by exceptional droughts and heatwaves, resulting in high
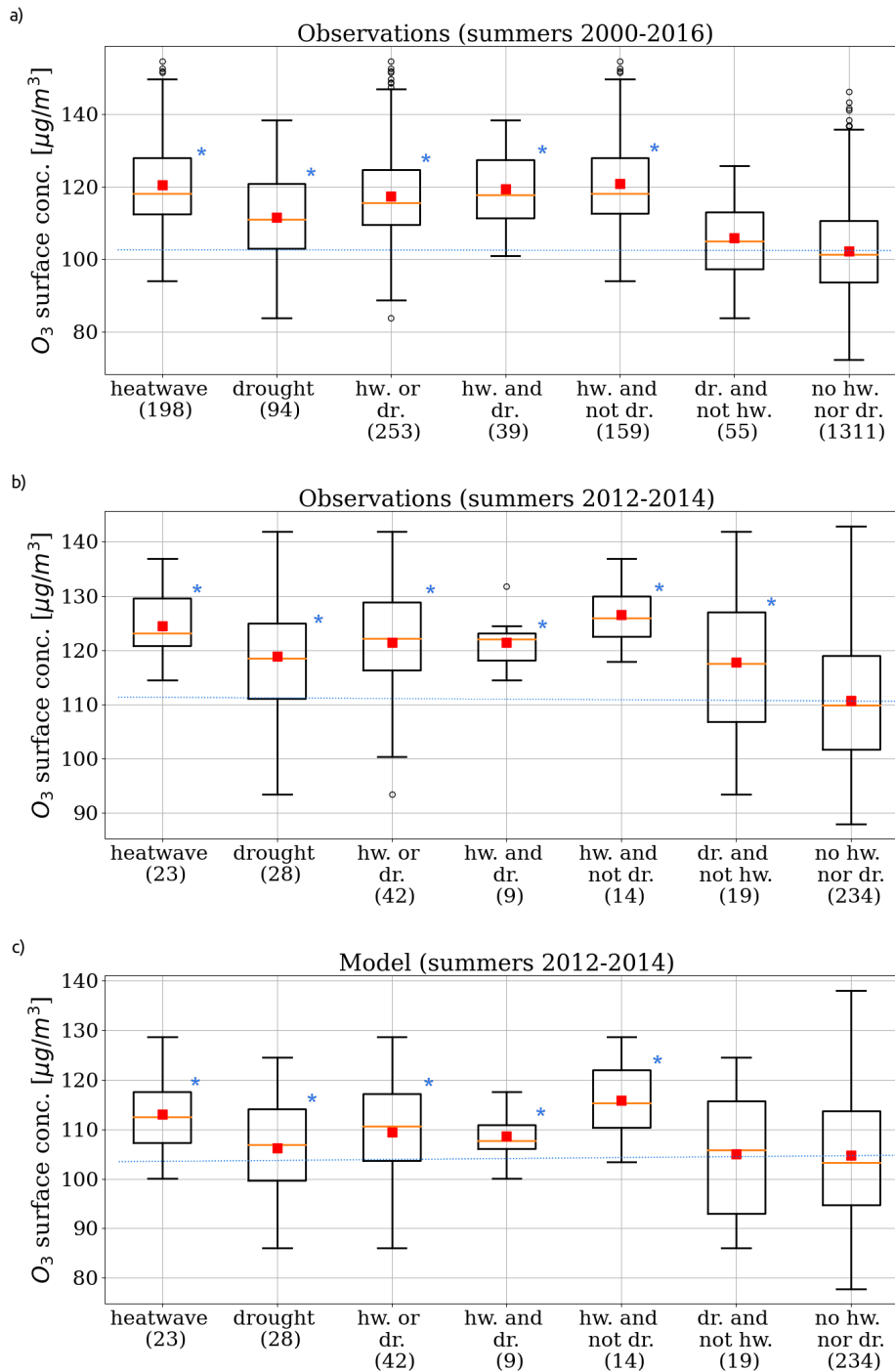
Figure 12. Same as Figure 10 with the observed surface O_3 concentration [$\mu g/m^3$] over the summers 2000-2016 (~~upper panel~~a) and 2012-2014 (~~middle panel~~b), and with the simulated surface O_3 ("all-emiss-dep" experiment) over the summers 2012-2014 (~~lower panel~~c).
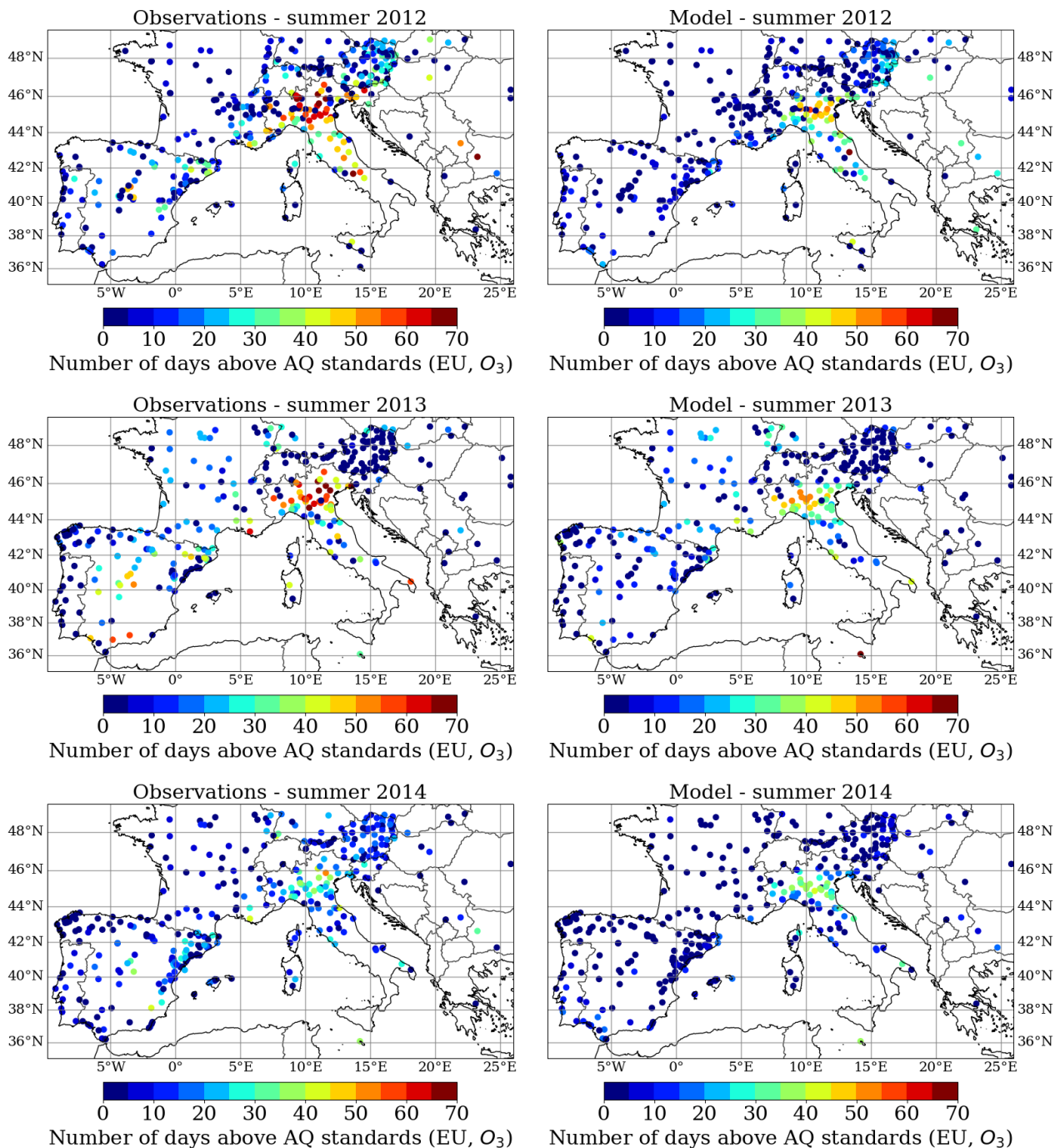
Figure 13. Number of days above the air quality threshold value from the European Union for surface O_3 (maximum daily 8 hour mean of 120 $\mu g/m^3$) over the summer 2012, 2013 and 2014 (JJA, 92 days in total). EEA observations (left column) are compared to CHIMERE ("all-emiss-dep") simulations (right column).

Table 4. Average percentage of stations with at least one exceedance day (first row) regarding EU standard during summer (JJA). Considering only those stations, the second row shows the average number of exceeding days per station and the lower rows the average distribution of days above the EU standard in function of extreme weather events. The mean exceedance concentration is indicated in parenthesis.

	EEA (2000-2016)	EEA (2012)	CHIMERE (2012)
Average fraction of stations (over all):	54%	61%	57%
Average number of exc. days / station:	27 days	28 days	18 days
Average distribution of exc. days:			
Normal conditions	52% ($+17\mu g/m^3$)	20% ($+15\mu g/m^3$)	21% ($+15\mu g/m^3$)
Heatwaves or droughts	48% ($+22\mu g/m^3$)	80% ($+18\mu g/m^3$)	79% ($+17\mu g/m^3$)
Heatwaves	34% ($+24\mu g/m^3$)	58% ($+20\mu g/m^3$)	65% ($+18\mu g/m^3$)
Isolated heatwaves	21% ($+24\mu g/m^3$)	16% ($+21\mu g/m^3$)	18% ($+16\mu g/m^3$)
Droughts	27% ($+18\mu g/m^3$)	64% ($+18\mu g/m^3$)	61% ($+17\mu g/m^3$)
Isolated droughts	14% ($+15\mu g/m^3$)	22% ($+14\mu g/m^3$)	14% ($+15\mu g/m^3$)

O_3 pollution. Around 80% of days above the EU threshold occurred during heatwaves or droughts for both observations and simulations.

6 Discussion and conclusions

The analyses presented in this study were organized around two main objectives. The first one was to assess the sensitivity of biogenic emissions, O_3 dry deposition and surface O_3 to the biomass decrease and soil dryness effect in a CTM model. The extremely dry summer 2012 was chosen and simulations were performed using the MEGAN v2.1 and CHIMERE v2020r1 model. We showed that the soil dryness parameter is critical during drought events, decreasing considerably the C_5H_8 emissions and O_3 dry deposition velocity. This effect has a larger impact than the biomass decrease. However, the resulting effect on surface O_3 remains limited.

In addition to the soil moisture activity factor used in MEGAN v2.1 that is mainly based on the wilting point (γ_{SM}), we proposed an innovative activity factor based on a soil water stress function (γ_{SWS}) simulated by the land surface and vegetation model ORCHIDEE. The latter induces a larger reduction of C_5H_8 emissions with more homogeneous patterns that follow the drought indicator. Furthermore, we adjusted this factor with a function fitted (γ_{SWSfit}) from experimental measurements in Bonn et al. (2019). By comparing the simulated surface concentration of C_5H_8 with observations at the Ersa measurement site (Corsica), γ_{SWSfit} showed promising results. However, such evaluation should be carried out over several sites and several years in order to determine with larger certainty the added value of this approach.

The second objective of this study was to quantify the variation of surface O_3 over the Southwestern Europe during agricul-

tural droughts, combined or not with heatwaves. Those extreme weather events were identified based on the RegIPSL model using the PLA indicator. During the 2000-2016 period, 59% of summer drought days were not accompanied by heatwaves (isolated droughts). For the summers 2012-2014, analyzed more specifically in this study, the 2m temperature is on average 5.5% lower during isolated droughts compared to all droughts, the shortwave radiation is 13.5% lower and the cloud fraction is 42% higher. As a result, surface O_3, but also BVOC emissions and O_3 dry deposition velocity, are substantially different if the drought considered is accompanied by a heatwave or not.

Based on a cluster approach using the PLA indicator, we showed that observed surface O_3 (summers 2000-2016) is larger by $+18\mu g/m^3$ in daily maximum during heatwaves and by $+9\mu g/m^3$ during droughts, compared to normal conditions. Despite a difference of several $\mu g/m^3$, CHIMERE correctly simulates the variations of O_3 concentration between the clusters of extreme events. The overall increase of surface O_3 during both heatwaves and droughts would be explained by O_3 precursor emission enhancement, O_3 dry deposition decrease and favorable weather conditions, so that all these mechanisms lead to an accumulation of O_3. However, we simulated a decrease of C_5H_8 emissions during isolated droughts, resulting in a non-significant difference of surface O_3 compared to normal conditions (from both observations and simulations). Despite a significant bias between the $HCHO$ total columns simulated by CHIMERE and observed by OMI, the satellite data confirm an average increase of $HCHO$ (+3% to +13% depending of the product considered) over our three regions of interest for all droughts and a decrease (-2% to -6%) for isolated droughts.

Finally, almost half of summer days (2000-2016 period) exceeding the EU standard of O_3 for air quality in Southwestern Europe occurred during droughts or heatwaves. However, this percentage can increase (up to 80%) for exceptionally dry and hot summers, like in 2012. Only 14% of the exceedance days occurred during isolated droughts.

The implementation of dynamical effects of droughts in the MEGAN - CHIMERE model contributes to a better representation of biosphere-atmosphere interactions. However, comparisons between simulated and observed surface O_3 still show large discrepancies. Important uncertainties appear to be related to BVOC emissions (especially due to the land cover classification), to NO_x concentrations for which CHIMERE presents limited performance scores of validation, to O_3 deposition and finally to meteorological conditions (e.g. temperature and PBLH). For instance, the simulated daily maximum temperature that is underestimated in the Northern Mediterranean compared to observations (see Sect. 4), may induced a decrease of O_3 precursors, especially as the emission–temperature relationship of BVOCs is exponential, with an optimal temperature for C_5H_8 species (Guenther et al., 1993). Such uncertainties need to be addressed to improve the simulation of O_3 during the summer, and especially over the Southwestern Europe.

In addition, the critical role of soil NO emissions in O_3 production is increasingly studied (e.g. Romer et al., 2018), especially in rural areas (e.g. Sha et al., 2021). As hydro-climatic conditions are critical for soil NO emissions, the O_3 budget during droughts and heatwaves is likely to be significantly influenced by soil NO emissions. In this study, dependence to soil dryness for NO emissions is not included. Emission pulses can occur when rain follows a drought and emission factors are higher with dry soil than with wet soil (Steinkamp and Lawrence, 2011; Weng et al., 2020).

Some recent knowledge on fundamental processes that allow a better representation of surface-atmosphere interactions during extreme weather events is not yet integrated by much, if not all, of the modelling community. Among the many examples

are the increased emission of monoterpenes and sesquiterpenes during the development of drought (e.g. Bonn et al., 2019; Peron et al., 2021) or the in-canopy chemistry that is ignored or approximated by the "big leaf" model approach (e.g. Clifton et al., 2020a). Several studies show that non-stomatal conductance in the Mediterranean counts as much as stomatal conductance in the O_3 sink budget (e.g. Gerosa et al., 2009; Sun et al., 2022). Moreover, non-stomatal conductance also seems to be significantly affected during droughts and heatwaves. In contrast to stomatal conductance, droughts and heatwaves should have opposite effects: an increase in non-stomatal conductance during heatwaves and a decrease during droughts (Wong et al., 2022). However, such changes are not taken into account in the EMEP deposition scheme implemented in CHIMERE. There is a real need for a better representation of stomatal conductance in deposition schemes.

In conclusion, we provide in this paper a detailed analysis of the drought and heatwave effects on modeled biosphere-troposphere interactions controlling surface O_3 concentration, supported by several observational data sets. Heatwaves, and droughts in a lower extent, induce a significant increase of the surface O_3. Soil dryness and biomass decrease, as specific effects of droughts, are critical for the variation of C_5H_8 emissions and O_3 dry deposition over the Southwestern Europe. We emphasize the need for a more dynamical representation of interactions between vegetation, meteorology and atmospheric chemistry in models in order to improve the simulation of summer O_3.

Acknowledgements. This work was granted access to the HPC resources of TGCC under allocation 10274 made by GENCI (Grand Equipement National de Calcul Intensif) and funded by Sorbonne Université (SU) and the Centre National d'Etudes Spatiales (CNES). We acknowledge the EEA to provide the AQ e-Reporting data set and Guillaume Siour for the data extraction and preparation. The MCD153AH and OMH-CHOd products were retrieved from the NASA EOSDIS Land Processes Distributed Active Archive Center (LPDAAC) and USGS Earth Resources Observation and Science (EROS) Center. Finally, we acknowledge the NCEP for the reanalysis meteorological data and the Norwegian Institute for Air Research (NILU) for the EBAS database.

Data availability. The data set of indicators of heatwaves and agricultural droughts ($PLA_{T2m/SD}$) is freely available at https://thredds-x.ipsl.fr/thredds/catalog/HyMeX/medcordex/data/Droughts_Heatwaves_1979_2016/catalog.html. The data from AQ e-Reporting can be found at https://www.eea.europa.eu/data-and-maps/data/aqereporting-9/aq-ereporting-products, from MODIS and OMI instrument at https://lpdaac.usgs.gov/data/, from NCEP at http://www.ncep.noaa.gov, from EBAS at https://ebas.nilu.no/data-access/ and from EFDC at http://www.europe-fluxdata.eu/.

Competing interests. The authors declare no competing financial interest.

Author contributions. AG, ST and JP: Conceptualization. AG, ST, AC, JP, AE and JL: Methodology. AG: Visualization. AG and ST: Writing of the original draft. AG, ST, AC, JP, AE and JL: Review and editing. All authors have read and agreed to the final version of the manuscript.

References

Alfaro, S. C. and Gomes, L.: Modeling mineral aerosol production by wind erosion: Emission intensities and aerosol size distributions in source areas, Journal of Geophysical Research: Atmospheres, 106, 18 075–18 084, https://doi.org/10.1029/2000JD900339, 2001.

Anand, J. S., Anav, A., Vitale, M., Peano, D., Unger, N., Yue, X., Parker, R. J., and Boesch, H.: Ozone-induced gross primary productivity reductions over European forests inferred from satellite observations, preprint, Biogeochemistry: Land, https://doi.org/10.5194/bg-2021-125, 2021.

Anav, A., Proietti, C., Menut, L., Carnicelli, S., De Marco, A., and Paoletti, E.: Sensitivity of stomatal conductance to soil moisture: implications for tropospheric ozone, Atmospheric Chemistry and Physics, 18, 5747–5763, https://doi.org/10.5194/acp-18-5747-2018, 2018.

Bian, H. and Prather, M. J.: Fast-J2: Accurate Simulation of Stratospheric Photolysis in Global Chemical Models, p. 16, https://link.springer.com/content/pdf/10.1023/A:1014980619462.pdf, 2002.

Bigi, A., Ghermandi, G., and Harrison, R. M.: Analysis of the air pollution climate at a background site in the Po valley, J. Environ. Monit., 14, 552–563, https://doi.org/10.1039/C1EM10728C, 2012.

Bonn, B., Magh, R.-K., Rombach, J., and Kreuzwieser, J.: Biogenic isoprenoid emissions under drought stress: different responses for isoprene and terpenes, Biogeosciences, 16, 4627–4645, https://doi.org/10.5194/bg-16-4627-2019, 2019.

Cao, J., Situ, S., Hao, Y., Xie, S., and Li, L.: Enhanced summertime ozone and SOA from biogenic volatile organic compound (BVOC) emissions due to vegetation biomass variability during 1981–2018 in China, preprint, Gases/Atmospheric Modelling/Troposphere/Chemistry (chemical composition and reactions), https://doi.org/10.5194/acp-2021-675, 2021.

Chance, K.: OMI/Aura Formaldehyde (HCHO) Total Column Daily L3 Weighted Mean Global 0.1deg Lat/Lon Grid V003, 10.5067/Aura/OMI/DATA3010, 2019.

Chen, F. and Dudhia, J.: Coupling an Advanced Land Surface–Hydrology Model with the Penn State–NCAR MM5 Modeling System. Part I: Model Implementation and Sensitivity, Monthly Weather Review, 129, 569–585, https://doi.org/10.1175/1520-0493(2001)129<0569:CAALSH>2.0.CO;2, 2001.

Chen, W. H., Guenther, A. B., Wang, X. M., Chen, Y. H., Gu, D. S., Chang, M., Zhou, S. Z., Wu, L. L., and Zhang, Y. Q.: Regional to Global Biogenic Isoprene Emission Responses to Changes in Vegetation From 2000 to 2015, Journal of Geophysical Research, p. 15, 2018.

Cheng, S., Huang, J., Ji, F., and Lin, L.: Uncertainties of soil moisture in historical simulations and future projections, Journal of Geophysical Research: Atmospheres, 122, 2239–2253, https://doi.org/10.1002/2016JD025871, 2017.

Chin, M., Ginoux, P., Kinne, S., Torres, O., Holben, B. N., Duncan, B. N., Martin, R. V., Logan, J. A., Higurashi, A., and Nakajima, T.: Tropospheric Aerosol Optical Thickness from the GOCART Model and Comparisons with Satellite and Sun Photometer Measurements, Journal of the Atmospheric Sciences, 59, 461–483, https://doi.org/10.1175/1520-0469(2002)059<0461:TAOTFT>2.0.CO;2, 2002.

Chu, Y., Li, J., Li, C., Tan, W., Su, T., and Li, J.: Seasonal and diurnal variability of planetary boundary layer height in Beijing: Intercomparison between MPL and WRF results, Atmospheric Research, 227, 1–13, https://doi.org/10.1016/j.atmosres.2019.04.017, 2019.

Clifton, O. E., Fiore, A. M., Massman, W. J., Baublitz, C. B., Coyle, M., Emberson, L., Fares, S., Farmer, D. K., Gentine, P., Gerosa, G., Guenther, A. B., Helmig, D., Lombardozzi, D. L., Munger, J. W., Patton, E. G., Pusede, S. E., Schwede, D. B., Silva, S. J., Sörgel, M., Steiner, A. L., and Tai, A. P. K.: Dry Deposition of Ozone Over Land: Processes, Measurement, and Modeling, Reviews of Geophysics, 58, https://doi.org/10.1029/2019RG000670, 2020a.

Clifton, O. E., Paulot, F., Fiore, A. M., Horowitz, L. W., Correa, G., Baublitz, C. B., Fares, S., Goded, I., Goldstein, A. H., Gruening, C., Hogg, A. J., Loubet, B., Mammarella, I., Munger, J. W., Neil, L., Stella, P., Uddling, J., Vesala, T., and Weng, E.: Influence of Dynamic

Ozone Dry Deposition on Ozone Pollution, Journal of Geophysical Research: Atmospheres, 125, https://doi.org/10.1029/2020JD032398, 2020b.

770 Cornes, R. C., van der Schrier, G., van den Besselaar, E. J., and Jones, P. D.: An ensemble version of the E-OBS temperature and precipitation data sets, Journal of Geophysical Research: Atmospheres, 123, 9391–9409, https://doi.org/10.1029/2017JD028200, publisher: Wiley Online Library, 2018.

Couvidat, F., Bessagnet, B., Garcia-Vivanco, M., Real, E., Menut, L., and Colette, A.: Development of an inorganic and organic aerosol model (CHIMERE 2017 β v1.0): seasonal and spatial evaluation over Europe, Geoscientific Model Development, 11, 165–194,
775 https://doi.org/10.5194/gmd-11-165-2018, 2018.

Curci, G., Palmer, P. I., Kurosu, T. P., Chance, K., and Visconti, G.: Estimating European volatile organic compound emissions using satellite observations of formaldehyde from the Ozone Monitoring Instrument, Atmospheric Chemistry and Physics, 10, 11 501–11 517, https://doi.org/10.5194/acp-10-11501-2010, 2010.

De Andrés, J. M., Borge, R., de la Paz, D., Lumbreras, J., and Rodríguez, E.: Implementation of a module for risk of ozone impacts assessment
780 to vegetation in the Integrated Assessment Modelling system for the Iberian Peninsula. Evaluation for wheat and Holm oak, Environmental Pollution, 165, 25–37, https://doi.org/10.1016/j.envpol.2012.01.048, 2012.

de Rosnay, P., Polcher, J., Bruen, M., and Laval, K.: Impact of a physically based soil water flow and soil-plant interaction representation for modeling large-scale land surface processes, Journal of Geophysical Research: Atmospheres, 107, ACL 3–1–ACL 3–19, https://doi.org/10.1029/2001JD000634, 2002.

785 De Smedt, I., Stavrakou, T., Hendrick, F., Danckaert, T., Vlemmix, T., Pinardi, G., Theys, N., Lerot, C., Gielen, C., Vigouroux, C., Hermans, C., Fayt, C., Veefkind, P., Müller, J.-F., and Van Roozendael, M.: Diurnal, seasonal and long-term variations of global formaldehyde columns inferred from combined OMI and GOME-2 observations, Atmospheric Chemistry and Physics, 15, 12 519–12 545, https://doi.org/10.5194/acp-15-12519-2015, 2015.

Demetillo, M. A. G., Anderson, J. F., Geddes, J. A., Yang, X., Najacht, E. Y., Herrera, S. A., Kabasares, K. M., Kotsakis, A. E., Lerdau, M. T.,
790 and Pusede, S. E.: Observing Severe Drought Influences on Ozone Air Pollution in California, Environmental Science & Technology, 53, 4695–4706, https://doi.org/10.1021/acs.est.8b04852, 2019.

Derognat, C.: Effect of biogenic volatile organic compound emissions on tropospheric chemistry during the Atmospheric Pollution Over the Paris Area (ESQUIF) campaign in the Ile-de-France region, Journal of Geophysical Research, 108, 8560, https://doi.org/10.1029/2001JD001421, 2003.

795 EEA: Air quality in Europe — 2020 report, https://www.actu-environnement.com/media/pdf/36559.pdfa, european Environment Agency, 2020.

Ek, M. B., Mitchell, K. E., Lin, Y., Rogers, E., Grunmann, P., Koren, V., Gayno, G., and Tarpley, J. D.: Implementation of Noah land surface model advances in the National Centers for Environmental Prediction operational mesoscale Eta model, Journal of Geophysical Research: Atmospheres, 108, 2002JD003 296, https://doi.org/10.1029/2002JD003296, 2003.

800 Emberson, L., Simpson, D., Tuovinen, J.-P., Ashmore, M., and Cambridge, H.: Towards a model of ozone deposition and stomatal uptake over Europe, Research Note No. 42, Norwegian Meteorological Institute, emep/msc-w edn., 2000.

Emmerson, K. M., Palmer, P. I., Thatcher, M., Haverd, V., and Guenther, A. B.: Sensitivity of isoprene emissions to drought over south-eastern Australia: Integrating models and satellite observations of soil moisture, Atmospheric Environment, 209, 112–124, https://doi.org/10.1016/j.atmosenv.2019.04.038, 2019.

Fares, S., Matteucci, G., Scarascia Mugnozza, G., Morani, A., Calfapietra, C., Salvatori, E., Fusaro, L., Manes, F., and Loreto, F.: Testing of models of stomatal ozone fluxes with field measurements in a mixed Mediterranean forest, Atmospheric Environment, 67, 242–251, https://doi.org/10.1016/j.atmosenv.2012.11.007, 2013.

Feng, Z., Yuan, X., Fares, S., Loreto, F., Li, P., Hoshika, Y., and Paoletti, E.: Isoprene is more affected by climate drivers than onoterpenes: A meta-analytic review on plant isoprenoid emissions, Pland, Cell & Environment, 42, 1939–1949, https://doi.org/https://doi.org/10.1111/pce.13535, 2019.

Friedl, M. A., Sulla-Menashe, D., Tan, B., Schneider, A., Ramankutty, N., Sibley, A., and Huang, X.: MODIS Collection 5 global land cover: Algorithm refinements and characterization of new datasets, Remote sensing of Environment, 114, 168–182, https://doi.org/10.1016/j.rse.2009.08.016, publisher: Elsevier, 2010.

García-Vila, M., Lorite, I., Soriano, M., and Fereres, E.: Management trends and responses to water scarcity in an irrigation scheme of Southern Spain, Agricultural Water Management, 95, 458–468, https://doi.org/10.1016/j.agwat.2007.11.009, 2008.

Gaubert, B., Coman, A., Foret, G., Meleux, F., Ung, A., Rouil, L., Ionescu, A., Candau, Y., and Beekmann, M.: Regional scale ozone data assimilation using an ensemble Kalman filter and the CHIMERE chemical transport model, Geoscientific Model Development, 7, 283–302, https://doi.org/10.5194/gmd-7-283-2014, 2014.

Gerosa, G., Finco, A., Mereu, S., Vitale, M., Manes, F., and Denti, A. B.: Comparison of seasonal variations of ozone exposure and fluxes in a Mediterranean Holm oak forest between the exceptionally dry 2003 and the following year, Environmental Pollution, 157, 1737–1744, https://doi.org/10.1016/j.envpol.2007.11.025, 2009.

Gong, C., Lei, Y., Ma, Y., Yue, X., and Liao, H.: Ozone–vegetation feedback through dry deposition and isoprene emissions in a global chemistry–carbon–climate model, Atmospheric Chemistry and Physics, 20, 3841–3857, https://doi.org/10.5194/acp-20-3841-2020, 2020.

González Abad, G., Liu, X., Chance, K., Wang, H., Kurosu, T. P., and Suleiman, R.: Updated Smithsonian Astrophysical Observatory Ozone Monitoring Instrument (SAO OMI) formaldehyde retrieval, Atmospheric Measurement Techniques, 8, 19–32, https://doi.org/10.5194/amt-8-19-2015, 2015.

Greve, P., Warrach-Sagi, K., and Wulfmeyer, V.: Evaluating Soil Water Content in a WRF-Noah Downscaling Experiment, Journal of Applied Meteorology and Climatology, 52, 2312–2327, https://doi.org/10.1175/JAMC-D-12-0239.1, 2013.

Guenther, A., Karl, T., Harley, P., Wiedinmyer, C., Palmer, P. I., and Geron, C.: Estimates of global terrestrial isoprene emissions using MEGAN (Model of Emissions of Gases and Aerosols from Nature), Atmos. Chem. Phys., p. 31, 2006.

Guenther, A. B., Zimmerman, P. R., Harley, P. C., Monson, R. K., and Fall, R.: Isoprene and monoterpene emission rate variability: Model evaluations and sensitivity analyses, Journal of Geophysical Research, 98, 12 609, https://doi.org/10.1029/93JD00527, 1993.

Guenther, A. B., Jiang, X., Heald, C. L., Sakulyanontvittaya, T., Duhl, T., Emmons, L. K., and Wang, X.: The Model of Emissions of Gases and Aerosols from Nature version 2.1 (MEGAN2.1): an extended and updated framework for modeling biogenic emissions, Geoscientific Model Development, 5, 1471–1492, https://doi.org/10.5194/gmd-5-1471-2012, 2012.

Guion, A., Turquety, S., Polcher, J., Pennel, R., Bastin, S., and Arsouze, T.: Droughts and heatwaves in the Western Mediterranean: impact on vegetation and wildfires using the coupled WRF-ORCHIDEE regional model (RegIPSL), Climate Dynamics, https://doi.org/10.1007/s00382-021-05938-y, 2021.

Hauglustaine, D. A., Balkanski, Y., and Schulz, M.: A global model simulation of present and future nitrate aerosols and their direct radiative forcing of climate, preprint, Aerosols/Atmospheric Modelling/Troposphere/Chemistry (chemical composition and reactions), https://doi.org/10.5194/acpd-14-6863-2014, 2014.

Haworth, M., Catola, S., Marino, G., Brunetti, C., Michelozzi, M., Riggi, E., Avola, G., Cosentino, S. L., Loreto, F., and Centritto, M.: Moderate Drought Stress Induces Increased Foliar Dimethylsulphoniopropionate (DMSP) Concentration and Isoprene Emission in Two Contrasting Ecotypes of Arundo donax, Frontiers in Plant Science, 8, 1016, https://doi.org/10.3389/fpls.2017.01016, 2017.

845 Hodnebrog, Ø., Solberg, S., Stordal, F., Svendby, T. M., Simpson, D., Gauss, M., Hilboll, A., Pfister, G. G., Turquety, S., Richter, A., Burrows, J. P., and Denier van der Gon, H. A. C.: Impact of forest fires, biogenic emissions and high temperatures on the elevated Eastern Mediterranean ozone levels during the hot summer of 2007, Atmospheric Chemistry and Physics, 12, 8727–8750, https://doi.org/10.5194/acp-12-8727-2012, 2012.

Huang, M., Crawford, J. H., Carmichael, G. R., Bowman, K. W., Kumar, S. V., and Sweeney, C.: Satellite soil moisture data assimila-
850 tion impacts on modeling weather variables and ozone in the southeastern US – Part 2: Sensitivity to dry-deposition parameterizations, Atmospheric Chemistry and Physics, 22, 7461–7487, https://doi.org/10.5194/acp-22-7461-2022, 2022.

Jacob, D. J.: Introduction to atmospheric chemistry, princeton university press. edn., 1999.

Jaén, C., Udina, M., and Bech, J.: Analysis of two heat wave driven ozone episodes in Barcelona and surrounding region: Meteorological and photochemical modeling, Atmospheric Environment, 246, 118 037, https://doi.org/10.1016/j.atmosenv.2020.118037, 2021.

855 Jerrett, M., Burnett, R. T., Pope, C. A., Ito, K., Thurston, G., Krewski, D., Shi, Y., Calle, E., and Thun, M.: Long-Term Ozone Exposure and Mortality, New England Journal of Medicine, 360, 1085–1095, https://doi.org/10.1056/NEJMoa0803894, 2009.

Jiang, X., Guenther, A., Potosnak, M., Geron, C., Seco, R., Karl, T., Kim, S., Gu, L., and Pallardy, S.: Isoprene emission response to drought and the impact on global atmospheric chemistry, Atmospheric Environment, 183, 69–83, https://doi.org/10.1016/j.atmosenv.2018.01.026, 2018.

860 Kavassalis, S. C. and Murphy, J. G.: Understanding ozone-meteorology correlations: A role for dry deposition: Ozone-Meteorology Correlations: Dry Dep, Geophysical Research Letters, 44, 2922–2931, https://doi.org/10.1002/2016GL071791, 2017.

Lamsal, L. N., Martin, R. V., van Donkelaar, A., Steinbacher, M., Celarier, E. A., Bucsela, E., Dunlea, E. J., and Pinto, J. P.: Ground-level nitrogen dioxide concentrations inferred from the satellite-borne Ozone Monitoring Instrument, Journal of Geophysical Research, 113, D16 308, https://doi.org/10.1029/2007JD009235, 2008.

865 Levelt, P., van den Oord, G., Dobber, M., Malkki, A., Huib Visser, Johan de Vries, Stammes, P., Lundell, J., and Saari, H.: The ozone monitoring instrument, IEEE Transactions on Geoscience and Remote Sensing, 44, 1093–1101, https://doi.org/10.1109/TGRS.2006.872333, 2006.

Levelt, P. F., Joiner, J., Tamminen, J., Veefkind, J. P., Bhartia, P. K., Stein Zweers, D. C., Duncan, B. N., Streets, D. G., Eskes, H., van der A, R., McLinden, C., Fioletov, V., Carn, S., de Laat, J., DeLand, M., Marchenko, S., McPeters, R., Ziemke, J., Fu, D., Liu, X., Pickering,
870 K., Apituley, A., González Abad, G., Arola, A., Boersma, F., Chan Miller, C., Chance, K., de Graaf, M., Hakkarainen, J., Hassinen, S., Ialongo, I., Kleipool, Q., Krotkov, N., Li, C., Lamsal, L., Newman, P., Nowlan, C., Suleiman, R., Tilstra, L. G., Torres, O., Wang, H., and Wargan, K.: The Ozone Monitoring Instrument: overview of 14 years in space, Atmospheric Chemistry and Physics, 18, 5699–5745, https://doi.org/10.5194/acp-18-5699-2018, 2018.

Lhotka, O. and Kyselý, J.: Characterizing joint effects of spatial extent, temperature magnitude and duration of heat waves and cold spells
875 over Central Europe, International Journal of Climatology, 35, 1232–1244, https://doi.org/10.1002/joc.4050, 2015.

Lin, M., Malyshev, S., Shevliakova, E., Paulot, F., Horowitz, L. W., Fares, S., Mikkelsen, T. N., and Zhang, L.: Sensitivity of Ozone Dry Deposition to Ecosystem-Atmosphere Interactions: A Critical Appraisal of Observations and Simulations, Global Biogeochemical Cycles, 33, 1264–1288, https://doi.org/10.1029/2018GB006157, 2019.

Lin, M., Horowitz, L., Xie, Y., Paulot, F., Malyshev, S., Shevliakova, E., Finco, A., Gerosa, G., Kubistin, D., and Pilegaard, K.: Vegetation feedbacks during drought exacerbate ozone air pollution extremes in Europe, Nature Climate Change, 10, https://doi.org/https://doi.org/10.1038/s41558-020-0743-y, 2020.

Liss, P. S. and Mervilat, L.: Air-Sea Gas Exchange Rates: Introduction and Synthesis, Springer Netherlands, Dordrecht, pp. 113–127, https://doi.org/10.1007/978-94-009-4738-2_5, 1986.

Maignan, F., Bréon, F.-M., Chevallier, F., Viovy, N., Ciais, P., Garrec, C., Trules, J., and Mancip, M.: Evaluation of a Global Vegetation Model using time series of satellite vegetation indices, Geoscientific Model Development, 4, 1103–1114, https://doi.org/10.5194/gmd-4-1103-2011, 2011.

Marticorena, B. and Bergametti, G.: Modeling the atmospheric dust cycle: 1. Design of a soil-derived dust emission scheme, Journal of Geophysical Research, 100, 16 415, https://doi.org/10.1029/95JD00690, 1995.

Menut, L., Bessagnet, B., Briant, R., Cholakian, A., Couvidat, F., Mailler, S., Pennel, R., Siour, G., Tuccella, P., Turquety, S., and Valari, M.: The CHIMERE v2020r1 online chemistry-transport model, preprint, Atmospheric sciences, https://doi.org/10.5194/gmd-2021-96, 2021.

Mertens, M., Kerkweg, A., Grewe, V., Jöckel, P., and Sausen, R.: Attributing ozone and its precursors to land transport emissions in Europe and Germany, Atmospheric Chemistry and Physics, 20, 7843–7873, https://doi.org/10.5194/acp-20-7843-2020, 2020.

Michou, M., Laville, P., Serça, D., Fotiadi, A., Bouchou, P., and Peuch, V.-H.: Measured and modeled dry deposition velocities over the ESCOMPTE area, Atmospheric Research, 74, 89–116, https://doi.org/10.1016/j.atmosres.2004.04.011, 2005.

Millet, D. B., Jacob, D. J., Turquety, S., Hudman, R. C., Wu, S., Fried, A., Walega, J., Heikes, B. G., Blake, D. R., Singh, H. B., Anderson, B. E., and Clarke, A. D.: Formaldehyde distribution over North America: Implications for satellite retrievals of formaldehyde columns and isoprene emission, Journal of Geophysical Research, 111, D24S02, https://doi.org/10.1029/2005JD006853, 2006.

Millet, D. B., Jacob, D. J., Boersma, K. F., Fu, T.-M., Kurosu, T. P., Chance, K., Heald, C. L., and Guenther, A.: Spatial distribution of isoprene emissions from North America derived from formaldehyde column measurements by the OMI satellite sensor, Journal of Geophysical Research, 113, D02 307, https://doi.org/10.1029/2007JD008950, 2008.

Miralles, D. G., Gentine, P., Seneviratne, S. I., and Teuling, A. J.: Land-atmospheric feedbacks during droughts and heatwaves: state of the science and current challenges, Annals of the New York Academy of Sciences, 1436, 19–35, https://doi.org/10.1111/nyas.13912, 2019.

Monahan, E.: In The Role of Air-Sea Exchange in Geochemical Cyclong, chap. The ocean as a source of atmospheric particles., Kluwer Academic Publishers, Dordrecht, Holland, pp. 129–163, 1986.

Müller, J.-F., Stavrakou, T., Wallens, S., De Smedt, I., Van Roozendael, M., Potosnak, M. J., Rinne, J., Munger, B., Goldstein, A., and Guenther, A. B.: Global isoprene emissions estimated using MEGAN, ECMWF analyses and a detailed canopy environment model, Atmos. Chem. Phys., 8, 1329–1341, https://acp.copernicus.org/articles/8/1329/2008/, 2008.

Myneni, R., Knyazikhin, Y., and Park, T.: MOD15A2H MODIS/terra leaf area index/FPAR 8-day L4 global 500 m SIN grid V006, NASA EOSDIS Land Processes DAAC, https://modis.gsfc.nasa.gov/data/dataprod/mod15.php, 2015.

Nuvolone, D., Petri, D., and Voller, F.: The effects of ozone on human heatlh, Environ Sci Pollut Res, pp. 8074–8088, https://doi.org/10.1007/s11356-017-9239-3, section: 25, 2018.

Opacka, B., Müller, J.-F., Stavrakou, T., Bauwens, M., Sindelarova, K., Markova, J., and Guenther, A. B.: Global and regional impacts of land cover changes on isoprene emissions derived from spaceborne data and the MEGAN model, Atmospheric Chemistry and Physics, 21, 8413–8436, https://doi.org/10.5194/acp-21-8413-2021, 2021.

915 Otero, N., Jurado, O., Butler, T., and Rust, H. W.: The impact of atmospheric blocking on the compounding effect of ozone pollution and temperature: A copula-based approach, preprint, Aerosols/Atmospheric Modelling/Troposphere/Chemistry (chemical composition and reactions), https://doi.org/10.5194/acp-2021-297, 2021.

Panthou, G., Vrac, M., Drobinski, P., Bastin, S., and Li, L.: Impact of model resolution and Mediterranean sea coupling on hydrometeorological extremes in RCMs in the frame of HyMeX and MED-CORDEX, Climate Dynamics, 51, 915–932, https://doi.org/10.1007/s00382-016-3374-2, 2018.

920 Perkins-Kirkpatrick, S. E. and Gibson, P. B.: Changes in regional heatwave characteristics as a function of increasing global temperature, Scientific Reports, 7, 12 256, https://doi.org/10.1038/s41598-017-12520-2, 2017.

Peron, A., Kaser, L., Fitzky, A. C., Graus, M., Halbwirth, H., Greiner, J., Wohlfahrt, G., Rewald, B., Sandén, H., and Karl, T.: Combined effects of ozone and drought stress on the emission of biogenic volatile organic compounds from Quercus robur L., Biogeosciences, 18, 535–556, https://doi.org/10.5194/bg-18-535-2021, 2021.

925 Porter, W. C. and Heald, C. L.: The mechanisms and meteorological drivers of the summertime ozone–temperature relationship, Atmospheric Chemistry and Physics, 19, 13 367–13 381, https://doi.org/10.5194/acp-19-13367-2019, 2019.

Potosnak, M. J., LeStourgeon, L., Pallardy, S. G., Hosman, K. P., Gu, L., Karl, T., Geron, C., and Guenther, A. B.: Observed and modeled ecosystem isoprene fluxes from an oak-dominated temperate forest and the influence of drought stress, Atmospheric Environment, 84, 930 314–322, https://doi.org/10.1016/j.atmosenv.2013.11.055, 2014.

Richards, N. A. D., Arnold, S. R., Chipperfield, M. P., Miles, G., Rap, A., Siddans, R., Monks, S. A., and Hollaway, M. J.: The Mediterranean summertime ozone maximum: global emission sensitivities and radiative impacts, Atmospheric Chemistry and Physics, 13, 2331–2345, https://doi.org/10.5194/acp-13-2331-2013, 2013.

Romer, P. S., Duffey, K. C., Wooldridge, P. J., Edgerton, E., Baumann, K., Feiner, P. A., Miller, D. O., Brune, W. H., Koss, A. R., de Gouw, 935 J. A., Misztal, P. K., Goldstein, A. H., and Cohen, R. C.: Effects of temperature-dependent NOx emissions on continental ozone production, Atmospheric Chemistry and Physics, 18, 2601–2614, https://doi.org/10.5194/acp-18-2601-2018, 2018.

Russo, S., Sillmann, J., and Fischer, E. M.: Top ten European heatwaves since 1950 and their occurrence in the coming decades, Environmental Research Letters, 10, 124 003, https://doi.org/10.1088/1748-9326/10/12/124003, 2015.

Ruti, P. M., Somot, S., Giorgi, F., Dubois, C., Flaounas, E., Obermann, A., Dell'Aquila, A., Pisacane, G., Harzallah, A., Lombardi, E., 940 Ahrens, B., Akhtar, N., Alias, A., Arsouze, T., Aznar, R., Bastin, S., Bartholy, J., Béranger, K., Beuvier, J., Bouffies-Cloché, S., Brauch, J., Cabos, W., Calmanti, S., Calvet, J.-C., Carillo, A., Conte, D., Coppola, E., Djurdjevic, V., Drobinski, P., Elizalde-Arellano, A., Gaertner, M., Galàn, P., Gallardo, C., Gualdi, S., Goncalves, M., Jorba, O., Jordà, G., L'Heveder, B., Lebeaupin-Brossier, C., Li, L., Liguori, G., Lionello, P., Maciàs, D., Nabat, P., Önol, B., Raikovic, B., Ramage, K., Sevault, F., Sannino, G., Struglia, M. V., Sanna, A., Torma, C., and Vervatis, V.: Med-CORDEX Initiative for Mediterranean Climate Studies, Bulletin of the American Meteorological Society, 97, 945 1187–1208, https://doi.org/10.1175/BAMS-D-14-00176.1, 2016.

Saunier, A., Ormeño, E., Boissard, C., Wortham, H., Temime-Roussel, B., Lecareux, C., Armengaud, A., and Fernandez, C.: Effect of mid-term drought on Quercus pubescens BVOCs' emission seasonality and their dependency on light and/or temperature, Atmospheric Chemistry and Physics, 17, 7555–7566, https://doi.org/10.5194/acp-17-7555-2017, 2017.

Sha, T., Ma, X., Zhang, H., Janechek, N., Wang, Y., Wang, Y., Castro García, L., Jenerette, G. D., and Wang, J.: Impacts of Soil NOx Emission 950 on O3 Air Quality in Rural California, Environmental Science & Technology, 55, 7113–7122, https://doi.org/10.1021/acs.est.0c06834, 2021.

Simpson, D., Fagerli, H., Jonson, J. E., Tsyro, S., Wind, P., and Tuovien, J. P.: Transboundary Acidification, Eutrophication and Ground Level Ozone in Europe. Part I: Unified EMEP Model Description, Technical report, Norwegian Meteorological Institute, 2003.

Simpson, D., Benedictow, A., Berge, H., Bergström, R., Emberson, L. D., Fagerli, H., Flechard, C. R., Hayman, G. D., Gauss, M., Jonson, J. E., Jenkin, M. E., Nyíri, A., Richter, C., Semeena, V. S., Tsyro, S., Tuovinen, J.-P., Valdebenito, Á., and Wind, P.: The EMEP MSC-W chemical transport model – technical description, Atmospheric Chemistry and Physics, 12, 7825–7865, https://doi.org/10.5194/acp-12-7825-2012, 2012.

Skamarock, W. C., Klemp, J. B., Dudhia, J., Gill, D. O., Barker, D. M., Wang, W., and Powers, J. G.: A description of the Advanced Research WRF version 3. NCAR/TN-475+STR, Tech. rep., University Corporation for Atmospheric Research, http://dx.doi.org/10.5065/D68S4MVH, 2008.

Spinoni, J., Naumann, G., Vogt, J. V., and Barbosa, P.: The biggest drought events in Europe from 1950 to 2012, Journal of Hydrology: Regional Studies, 3, 509–524, https://doi.org/10.1016/j.ejrh.2015.01.001, 2015.

Spinoni, J., Vogt, J. V., Naumann, G., Barbosa, P., and Dosio, A.: Will drought events become more frequent and severe in Europe?, International Journal of Climatology, 38, 1718–1736, https://doi.org/10.1002/joc.5291, 2018.

Stéfanon, M., D'Andrea, F., and Drobinski, P.: Heatwave classification over Europe and the Mediterranean region, Environmental Research Letters, 7, 014 023, https://doi.org/10.1088/1748-9326/7/1/014023, 2012.

Steinkamp, J. and Lawrence, M. G.: Improvement and evaluation of simulated global biogenic soil NO emissions in an AC-GCM, Atmospheric Chemistry and Physics, 11, 6063–6082, https://doi.org/10.5194/acp-11-6063-2011, 2011.

Stohl, A., Williams, E., Wotawa, G., and Kromp-Kolb, H.: A European inventory of soil nitric oxide emissions and the effect of these emissions on the photochemical formation of ozone, Atmospheric Environment, 30, 3741–3755, https://doi.org/10.1016/1352-2310(96)00104-5, 1996.

Sun, S., Tai, A. P. K., Yung, D. H. Y., Wong, A. Y. H., Ducker, J. A., and Holmes, C. D.: Influence of plant ecophysiology on ozone dry deposition: comparing between multiplicative and photosynthesis-based dry deposition schemes and their responses to rising CO2 level, Biogeosciences, 19, 1753–1776, https://doi.org/10.5194/bg-19-1753-2022, 2022.

Svoboda, M. D. and Fuchs, B. A.: Handbook of drought indicators and indices., Geneva, world meteorological organization and global water partnership edn., oCLC: 958433349, 2016.

Tai, A. P. K., Martin, M. V., and Heald, C. L.: Threat to future global food security from climate change and ozone air pollution, Nature Climate Change, 4, 817–821, https://doi.org/10.1038/nclimate2317, 2014.

Thompson, G. and Eidhammer, T.: A Study of Aerosol Impacts on Clouds and Precipitation Development in a Large Winter Cyclone, Journal of the Atmospheric Sciences, 71, 3636–3658, https://doi.org/10.1175/JAS-D-13-0305.1, 2014.

Thunis, P., Pernigotti, D., and Gerboles, M.: Model quality objectives based on measurement uncertainty. Part I: Ozone, Atmospheric Environment, 79, 861–868, https://doi.org/10.1016/j.atmosenv.2013.05.018, 2013.

Turquety, S., Menut, L., Siour, G., Mailler, S., Hadji-Lazaro, J., George, M., Clerbaux, C., Hurtmans, D., and Coheur, P.-F.: APIFLAME v2.0 biomass burning emissions model: impact of refined input parameters on atmospheric concentration in Portugal in summer 2016, Geoscientific Model Development, 13, 2981–3009, https://doi.org/10.5194/gmd-13-2981-2020, 2020.

Van Leer, B.: Towards the ultimate conservative difference scheme. IV. A new approach to numerical convection, Journal of Computational Physics, 23, 276–299, https://doi.org/10.1016/0021-9991(77)90095-X, 1977.

Vautard, R., Honore, C., Beekmann, M., and Rouil, L.: Simulation of ozone during the August 2003 heat wave and emission control scenarios, Atmospheric Environment, 39, 2957–2967, https://doi.org/10.1016/j.atmosenv.2005.01.039, 2005.

Vicente-Serrano, S. M.: Evaluating the impact of drought using remote sensing in a Mediterranean, semi-arid region, Natural Hazards, 40, 173–208, https://doi.org/10.1007/s11069-006-0009-7, publisher: Springer, 2007.

Vicente-Serrano, S. M., Beguería, S., and López-Moreno, J. I.: A Multiscalar Drought Index Sensitive to Global Warming: The Standardized Precipitation Evapotranspiration Index, Journal of Climate, 23, 1696–1718, https://doi.org/10.1175/2009JCLI2909.1, 2010.

Vicente-Serrano, S. M., Gouveia, C., Camarero, J. J., Beguería, S., Trigo, R., López-Moreno, J. I., Azorín-Molina, C., Pasho, E., Lorenzo-Lacruz, J., Revuelto, J., and others: Response of vegetation to drought time-scales across global land biomes, Proceedings of the National Academy of Sciences, 110, 52–57, https://doi.org/10.1073/pnas.1207068110, publisher: National Acad Sciences, 2013.

Wang, P., Liu, Y., Dai, J., Fu, X., Wang, X., Guenther, A., and Wang, T.: Isoprene Emissions Response to Drought and the Impacts on Ozone and SOA in China, Journal of Geophysical Research: Atmospheres, 126, https://doi.org/10.1029/2020JD033263, 2021a.

Wang, Y., Xie, Y., Dong, W., Ming, Y., Wang, J., and Shen, L.: Adverse effects of increasing drought on air quality via natural processes, Atmospheric Chemistry and Physics, 17, 12 827–12 843, https://doi.org/10.5194/acp-17-12827-2017, 2017.

Wang, Y., Tan, X., Huang, L., Wang, Q., Li, H., Zhang, H., Zhang, K., Liu, Z., Traore, D., Yaluk, E., Fu, J. S., and Li, L.: The impact of biogenic emissions on ozone formation in the Yangtze River Delta region based on MEGANv3.1, Air Quality, Atmosphere & Health, 14, 763–774, https://doi.org/10.1007/s11869-021-00977-0, 2021b.

Weng, H., Lin, J., Martin, R., Millet, D. B., Jaeglé, L., Ridley, D., Keller, C., Li, C., Du, M., and Meng, J.: Global high-resolution emissions of soil NOx, sea salt aerosols, and biogenic volatile organic compounds, Scientific Data, 7, 148, https://doi.org/10.1038/s41597-020-0488-5, 2020.

Wesely, M.: Parameterization of surface resistances to gaseous dry deposition in regional-scale numerical models, Atmospheric Environment, 41, 52–63, https://doi.org/10.1016/j.atmosenv.2007.10.058, 1989.

Wong, A. Y. H., Geddes, J. A., Ducker, J. A., Holmes, C. D., Fares, S., Goldstein, A. H., Mammarella, I., and Munger, J. W.: New Evidence for the Importance of Non-Stomatal Pathways in Ozone Deposition During Extreme Heat and Dry Anomalies, Geophysical Research Letters, 49, https://doi.org/10.1029/2021GL095717, 2022.

Yuan, H., Dai, Y., Xiao, Z., Ji, D., and Shangguan, W.: Reprocessing the MODIS Leaf Area Index products for land surface and climate modelling, Remote Sensing of Environment, 115, 1171–1187, https://doi.org/10.1016/j.rse.2011.01.001, 2011.

Zampieri, M., D'Andrea, F., Vautard, R., Ciais, P., de Noblet-Ducoudré, N., and Yiou, P.: Hot European summers and the role of soil moisture in the propagation of Mediterranean drought, Journal of Climate, 22, 4747–4758, https://doi.org/10.1175/2009JCLI2568.1, 2009.

Zhang, Q. J., Beekmann, M., Drewnick, F., Freutel, F., Schneider, J., Crippa, M., Prevot, A. S. H., Baltensperger, U., Poulain, L., Wiedensohler, A., Sciare, J., Gros, V., Borbon, A., Colomb, A., Michoud, V., Doussin, J.-F., Denier van der Gon, H. A. C., Haeffelin, M., Dupont, J.-C., Siour, G., Petetin, H., Bessagnet, B., Pandis, S. N., Hodzic, A., Sanchez, O., Honoré, C., and Perrussel, O.: Formation of organic aerosol in the Paris region during the MEGAPOLI summer campaign: evaluation of the volatility-basis-set approach within the CHIMERE model, Atmospheric Chemistry and Physics, 13, 5767–5790, https://doi.org/10.5194/acp-13-5767-2013, 2013.

Zhu, L., Jacob, D. J., Kim, P. S., Fisher, J. A., Yu, K., Travis, K. R., Mickley, L. J., Yantosca, R. M., Sulprizio, M. P., De Smedt, I., González Abad, G., Chance, K., Li, C., Ferrare, R., Fried, A., Hair, J. W., Hanisco, T. F., Richter, D., Jo Scarino, A., Walega, J., Weibring, P., and Wolfe, G. M.: Observing atmospheric formaldehyde (HCHO) from space: validation and intercomparison of six retrievals from four satellites (OMI, GOME2A, GOME2B,OMPS) with SEAC4RS aircraft observations over the southeast US, Atmospheric Chemistry and Physics, 16, 13 477–13 490, https://doi.org/10.5194/acp-16-13477-2016, 2016.

Zhu, L., Mickley, L. J., Jacob, D. J., Marais, E. A., Sheng, J., Hu, L., Abad, G. G., and Chance, K.: Long-term (2005-2014) trends in formaldehyde (HCHO) columns across North America as seen by the OMI satellite instrument: Evidence of changing emissions of volatile organic

compounds: HCHO Trend Across North America, Geophysical Research Letters, 44, 7079–7086, https://doi.org/10.1002/2017GL073859, 2017.
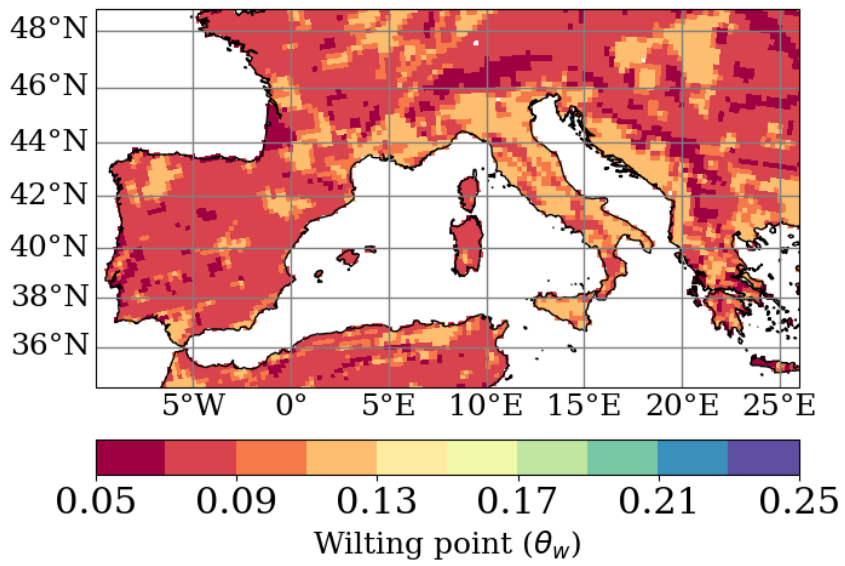
Figure S1. Wilting point parameter $[m^3/m^3]$ from Chen and Dudhia (2001) gridded over the Med-CORDEX domain with the USGS soil type map (STATSGO-FAO product).

1030 **Appendix: Supplementary Information**
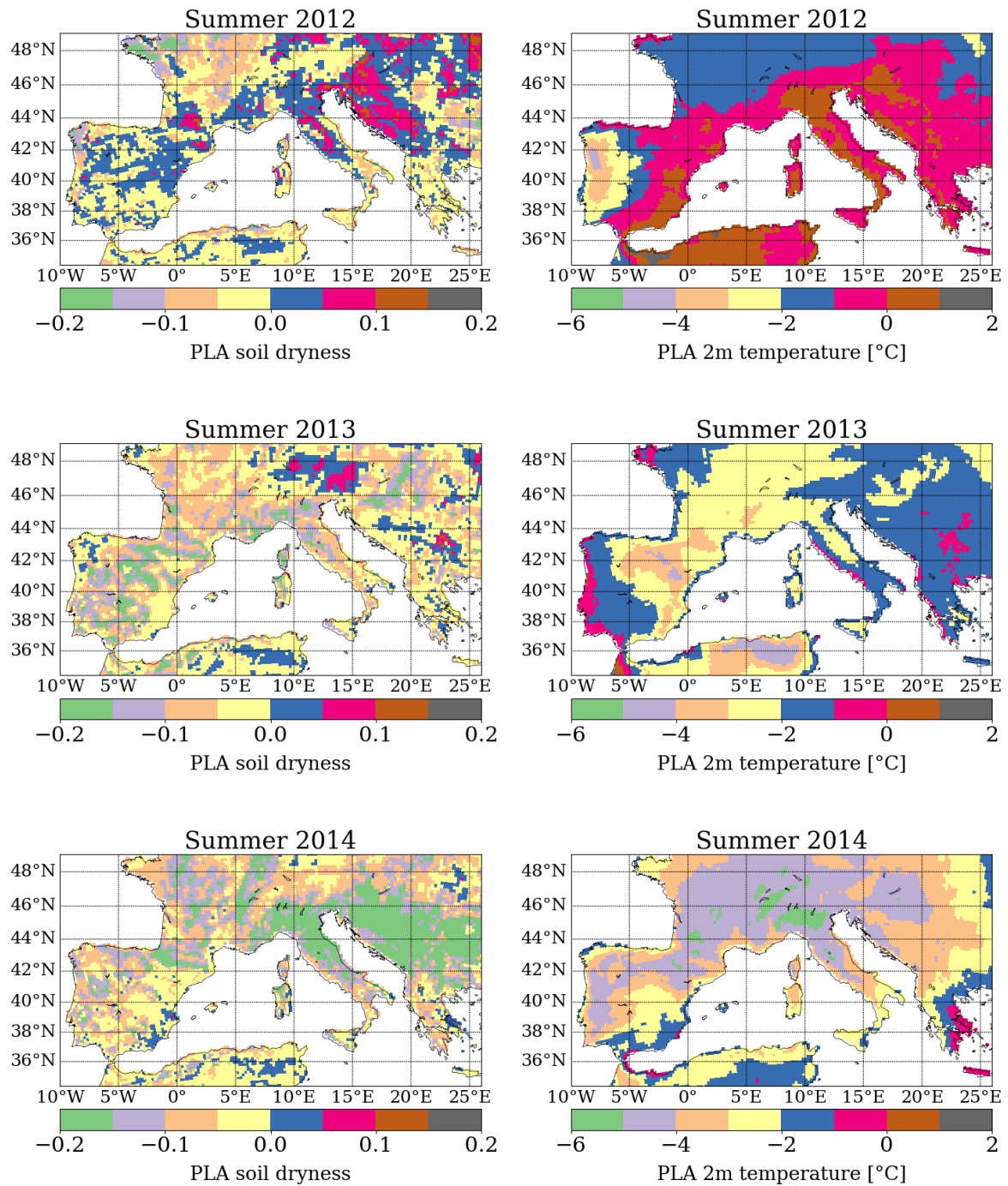
Figure S2. Summer mean (JJA) drought (PLA_{SD}) and heatwave indicators (PLA_{T2m}) for 2012, 2013 and 2014.
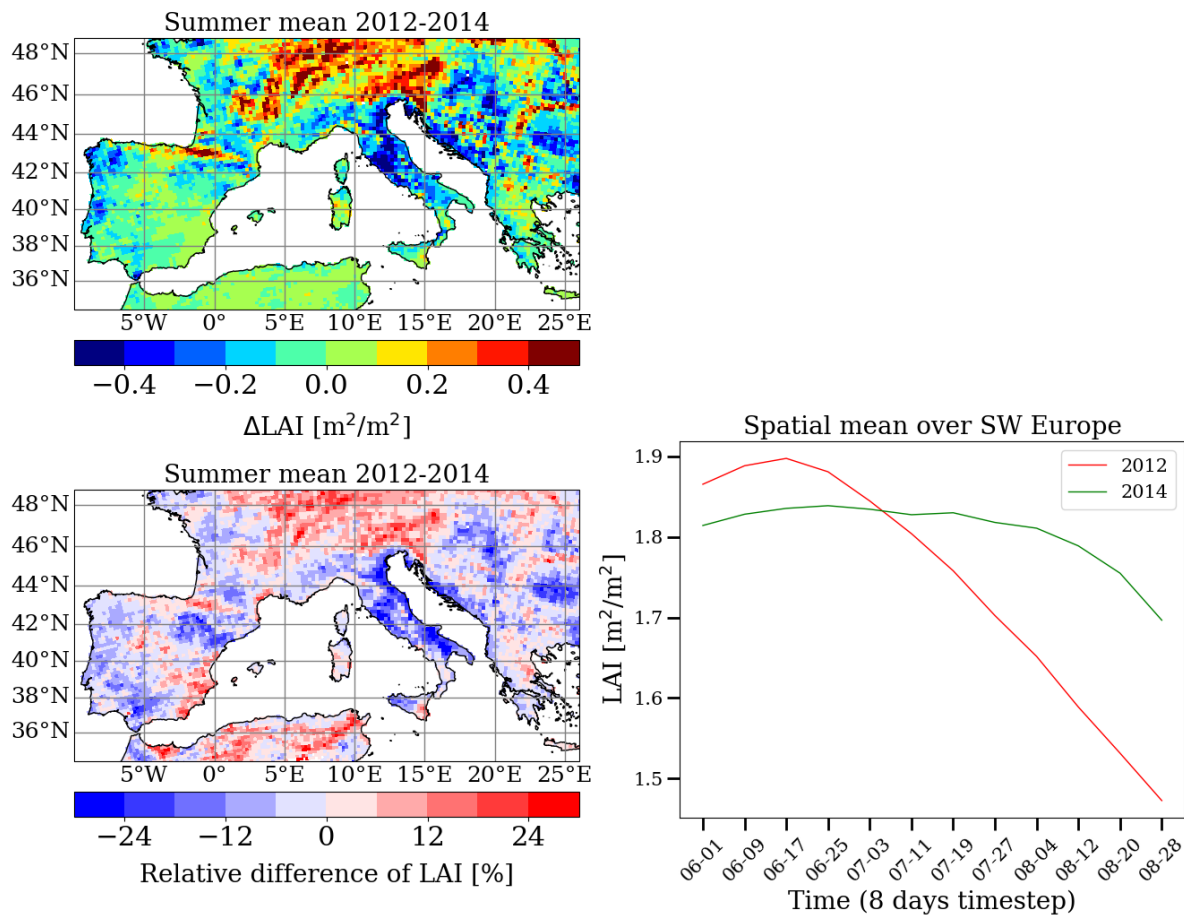
Figure S3. Mean ΔLAI $[m^2/m^2]$ between summer (JJA) 2012 and 2014 (upper left), relative difference of LAI (lower left) and time series of LAI spatially averaged over the Southwestern Europe (lower right).
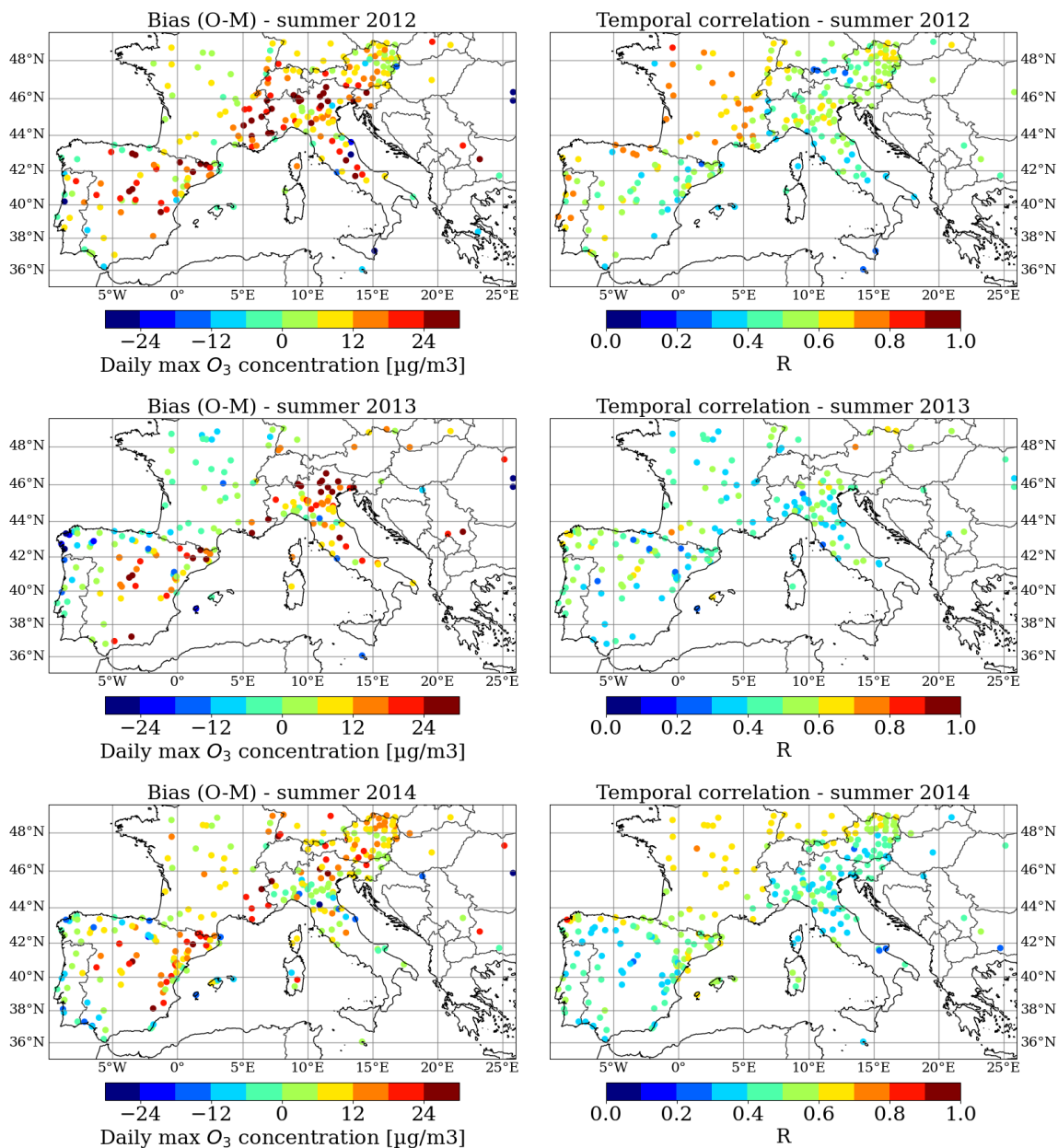
Figure S4. Validation scores of the daily maximum surface O_3 [$\mu g/m^3$] for summer (JJA) 2012, 2013 and 2014 ("Reference" simulations), with the European surface network observations AQ e-Reporting. Left column: mean bias. Right column: temporal correlation (R pearson). The number of stations taken into account is 167, 188 and 207 respectively for summer 2012, 2013 and 2014
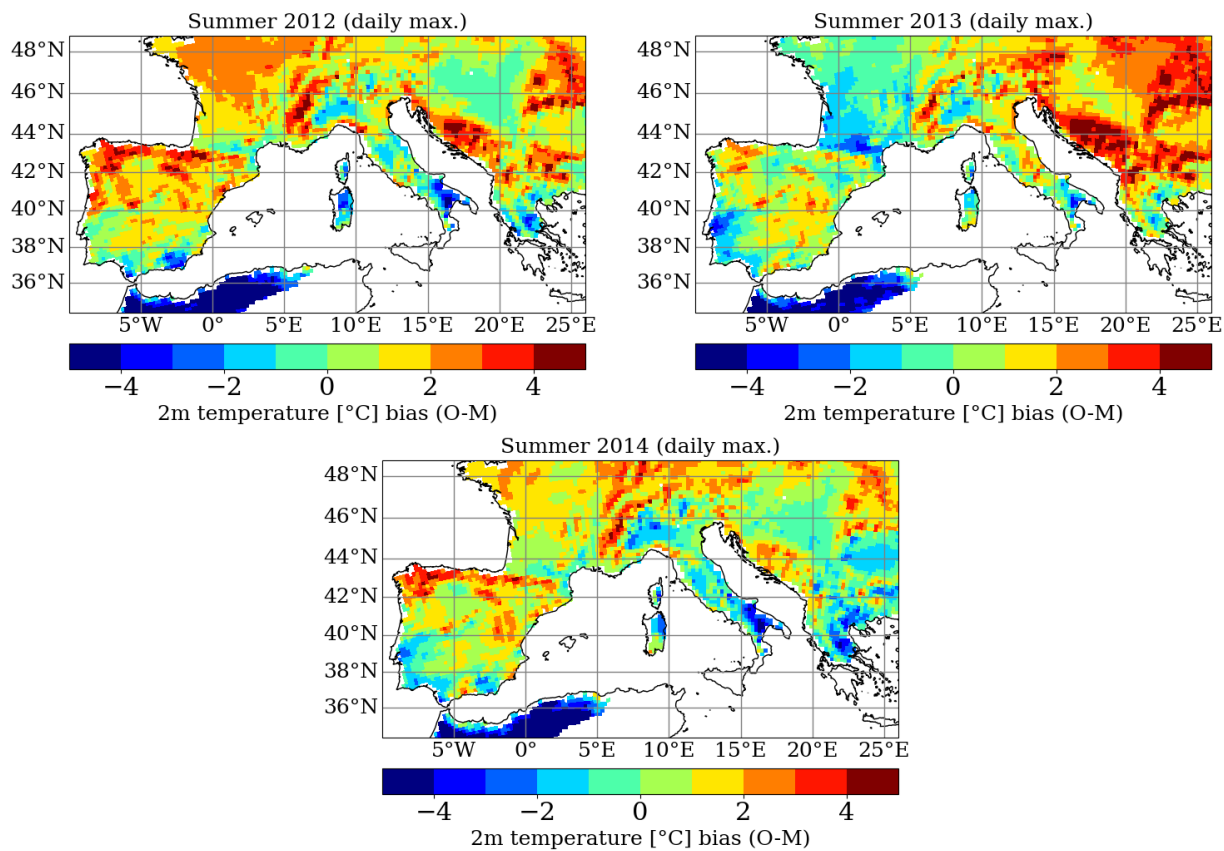
Figure S5. Summer mean bias (JJA) of the daily maximum 2m temperature between observations (E-OBS) and simulations (CHIMERE) for 2012, 2013 and 2014.
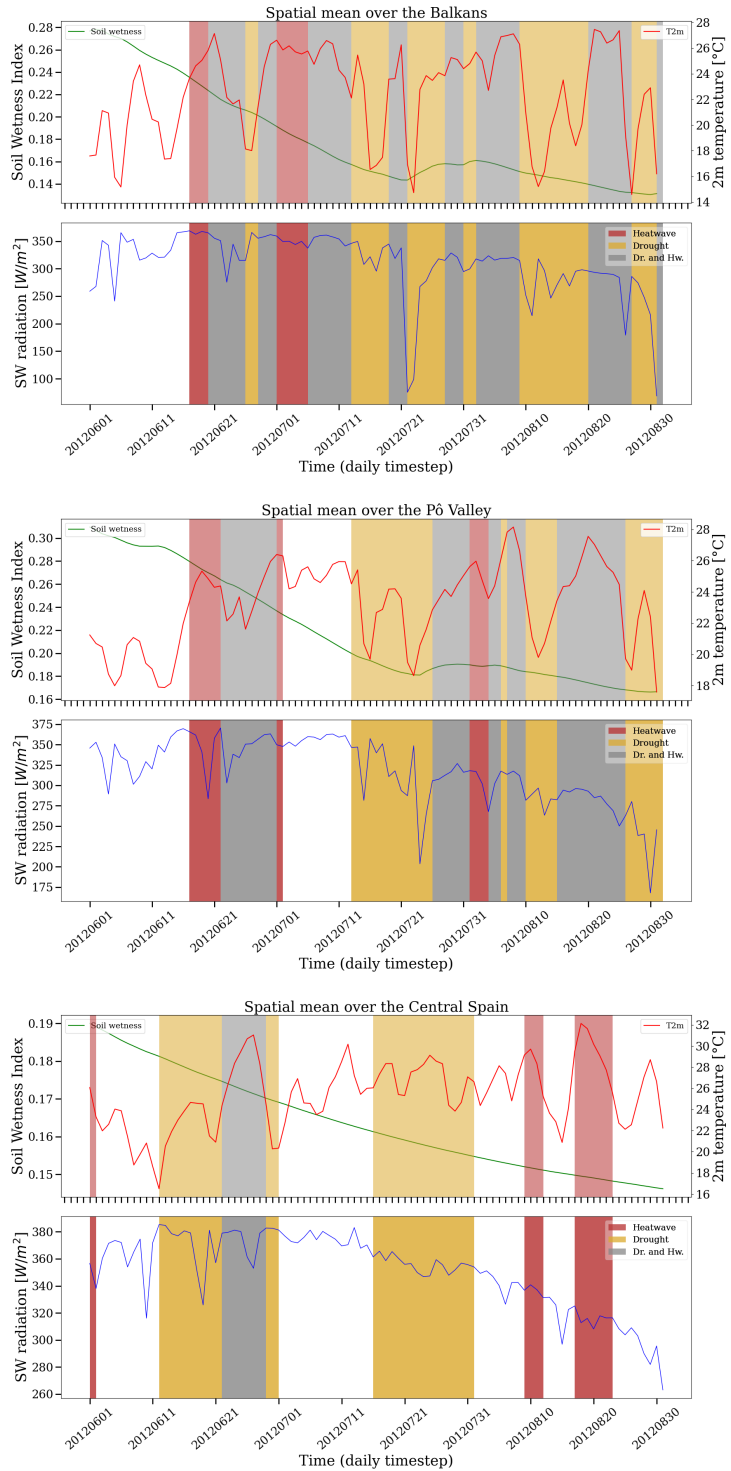
Figure S6. Daily mean 2m temperature, shortwave radiation and soil wetness simulated by the WRF model during summer 2012 over the Balkans (upper panel), Pô Valley (middle) and Central Spain (lower).
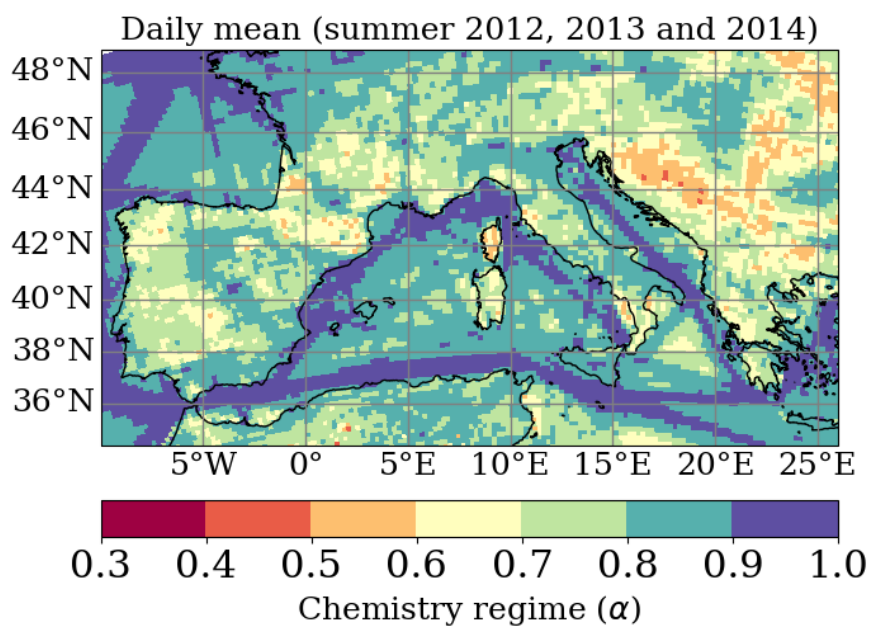
Figure S7. Daily mean chemistry regime parameter [α] averaged over the summer 2012, 2013 and 2014 ("Reference" simulations). α calculates the ratio of the reaction rate of RO_2 radicals with NO (high-NOx regime) with respect to the sum of reaction rates of the reactions with HO_2 and RO_2 (low-NOx regime). It gives a relative indication of low-NO_x (low α, about 0.5) and high-NO_x (high α, about 0.9) regime areas that are detailed in Zhang et al. (2013). More information about the calculation method of α is provided on the online documentation (https://www.lmd.polytechnique.fr/chimere/).
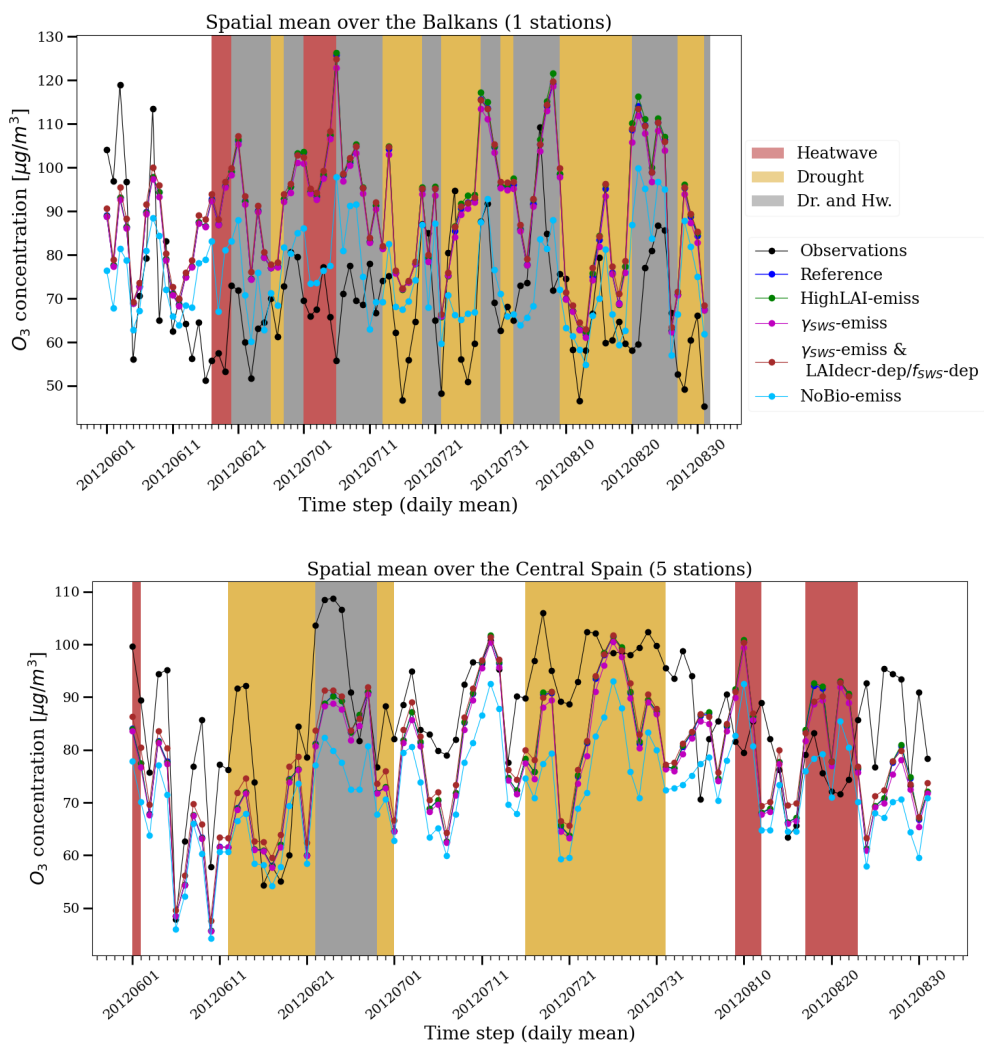
Figure S8. Daily mean O_3 surface concentration $[\mu g/m^3]$ during summer 2012, spatially averaged over the Balkans (upper panel) and Central Spain (lower panel) from the EEA observations and the different CHIMERE experiments.
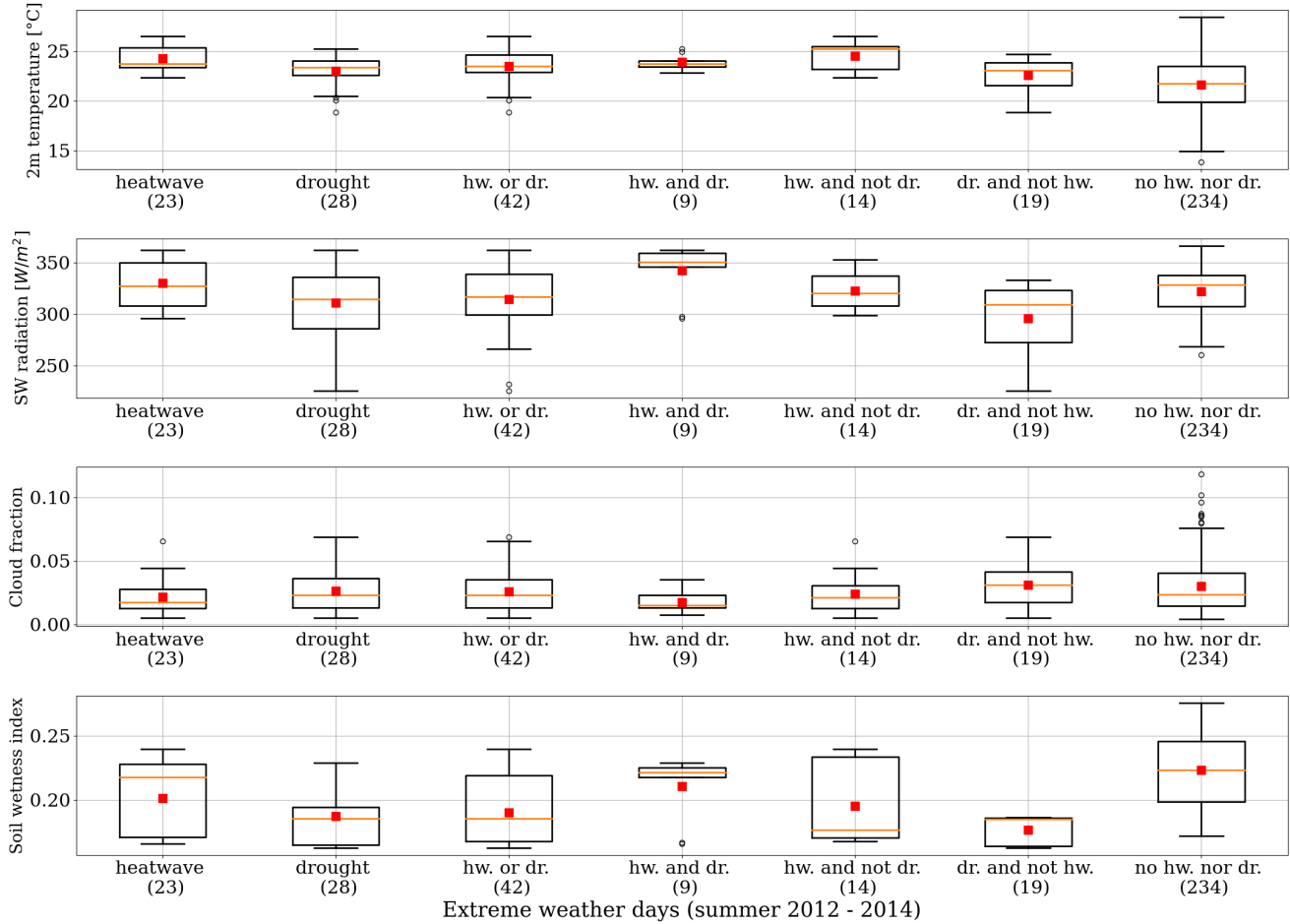
Figure S9. Simulated weather conditions (2m temperature, shortwave radiation, cloud fraction and soil wetness) by the WRF model over the Southwestern Europe, clustered by identified extreme weather events (from the RegIPSL model). The number of days is in parentheses. The analyzed period is summer 2012, 2013 and 2014, covering a total number of 276 days.
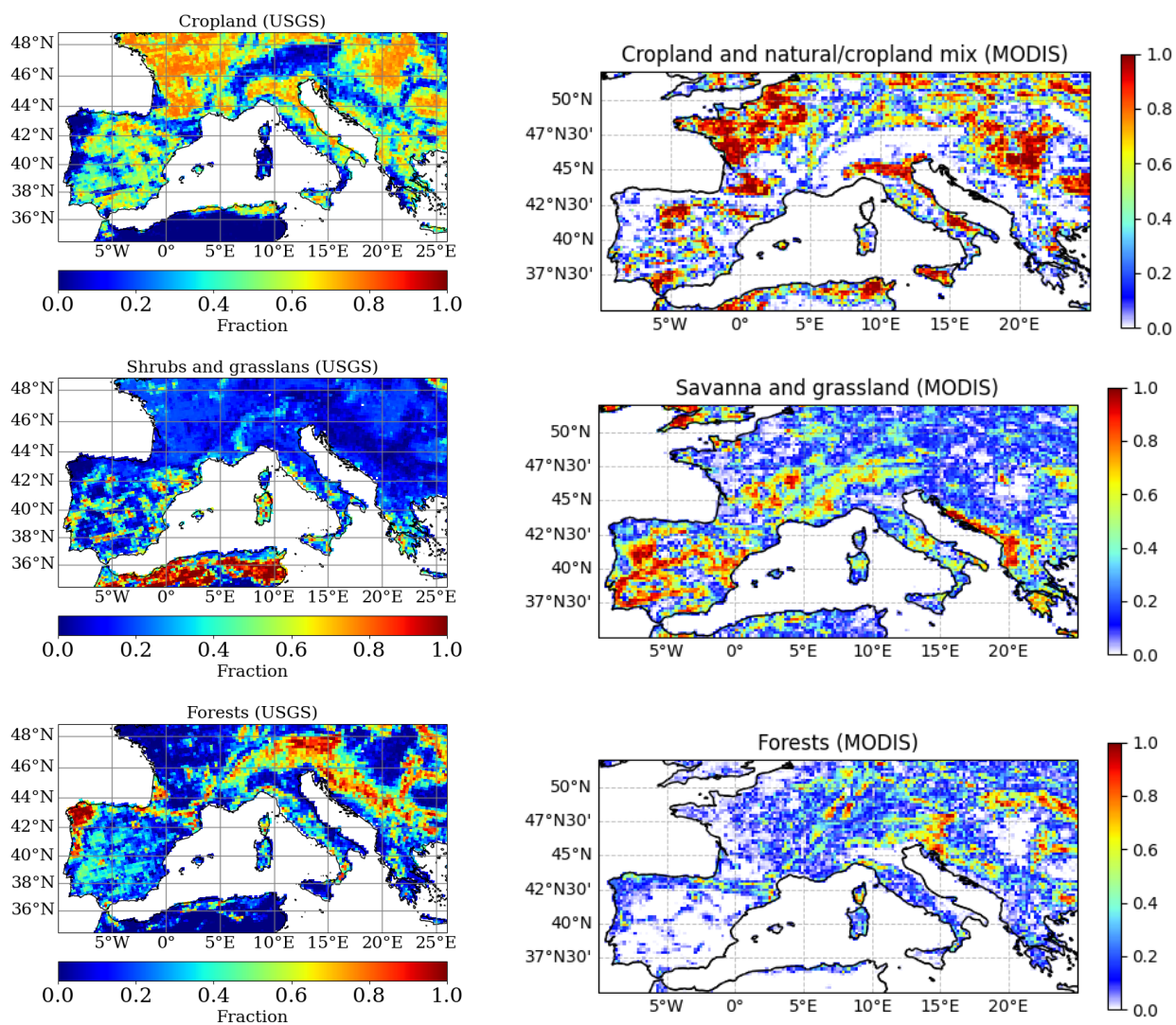
Figure S10. Land cover fraction of cropland, grassland and forests over the Southwestern Europe from USGS (left column) and MODIS MCD12 product (right column).
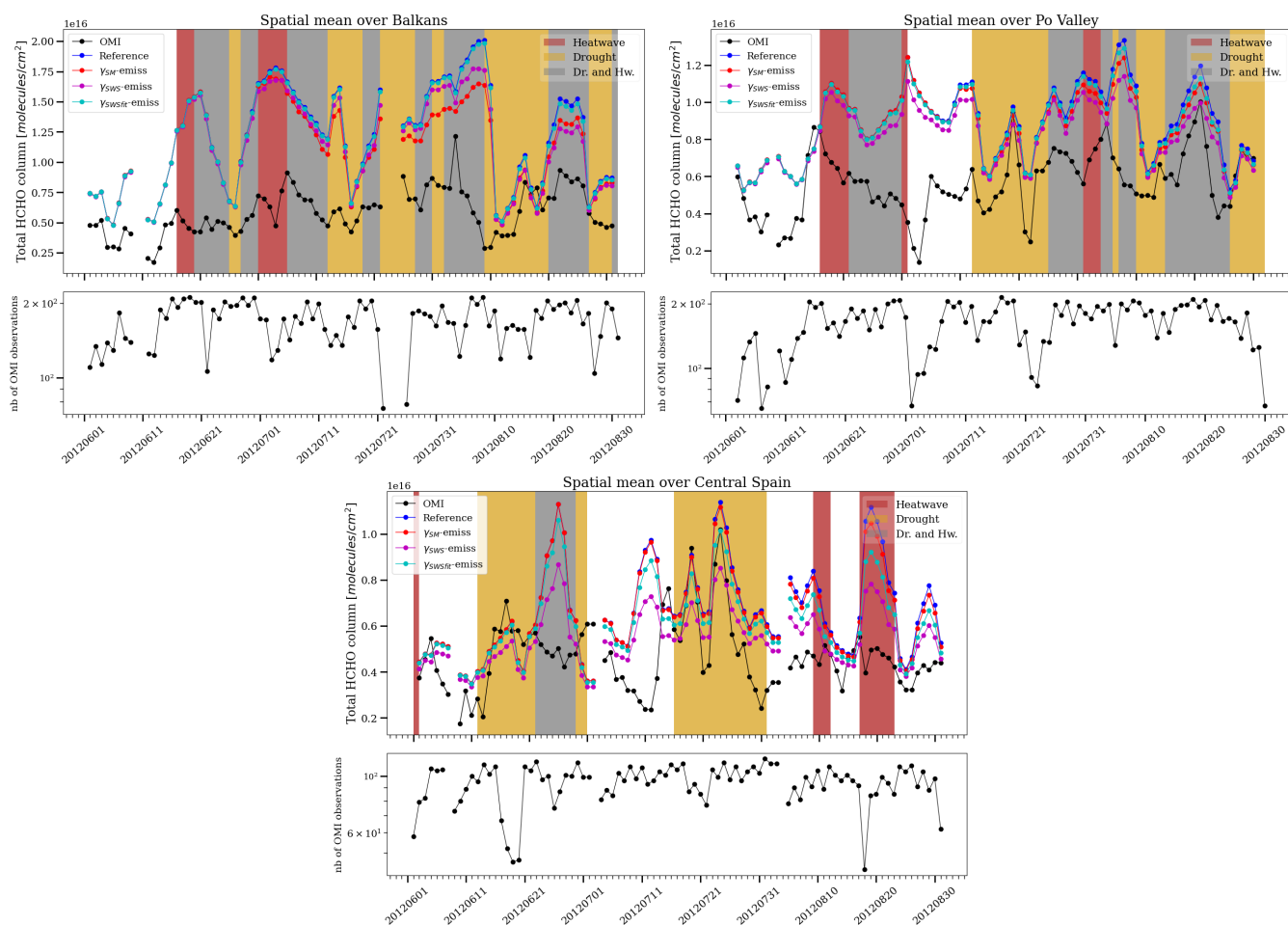
Figure S11. Daily HCHO total column [$molecules/cm^2$] during summer 2012 observed by OMI (OMHCHOd level 3 product) and simulated by CHIMERE, averaged over the Balkans (upper left panel), Pô Valley (upper right panel) and Central Spain (lower panel). A moving average window of 3 days is applied on observations and only days with at least 30% of data over the spatial cover are kept. The number of observations (OMI pixels) is indicated below each panel.